Structural and Functional Characterization of Ube2H, a Ubiquitin-Conjugating Enzyme with a C-terminal Extension

Dana E. Loutey

A thesis

submitted in partial fulfillment of the

requirements for the degree of

Master of Science

University of Washington

2019

Committee:

Rachel Klevit

William Zagotta

Ning Zheng

Andrea Wills

Justin Kollman

Program Authorized to Offer Degree:

Biochemistry

University of Washington

Abstract

Structural and Functional Characterization of Ube2H, a Ubiquitin-Conjugating Enzyme with a C-terminal Extension

Dana E. Loutey

Chair of the Supervisory Committee:

Rachel Klevit

Department of Biochemistry

The human proteome contains over forty ubiquitin-conjugating enzymes, each harboring a conserved core domain. Despite their structural similarities, E2s must discriminate between hundreds of E3 ligases to interact specifically with their cognate partners. Structural and functional characterization of E2s in the last few decades has revealed unique mechanistic details for each E2 studied thus far, but no universal rule appears to govern how E2 enzymes specifically recognize their cognate binding partners. Many E2s remain uncharacterized and promise to reveal novel strategies by which these apparently simple enzymes achieve specificity in both E3 binding and Ub transfer. Ube2H is a human E2 enzyme with an uncharacterized C-terminal extension of 32 residues. The extension is phylogenetically conserved, but its function is unknown. In this thesis, I employ biophysical and biochemical techniques to investigate the structural and biochemical function of Ube2H's C-terminal extension, both alone and in the presence of putative E3 ligases and binding partners.

TABLE OF CONTENTS

LIST OF FIGURES

Chapter 1. INTRODUCTION

1.1 THE UBIQUITIN SYSTEM

Protein homeostasis depends on regulated protein degradation by the ubiquitin proteasome system. In the ubiquitin cascade, the sequential action of E1-activating, E2-conjugating, and E3 ligase enzymes results in the covalent attachment of ubiquitin (Ub) onto protein substrates (Figure 1.1).

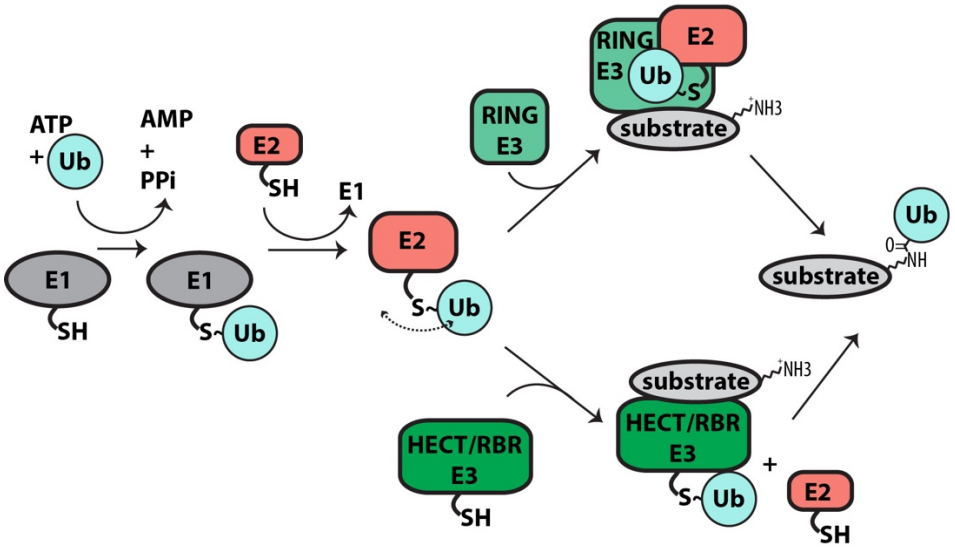

Figure 1.1. Schematic illustration of the ubiquitin cascade. E1-activating enzymes are charged with Ub at an active site cysteine in an ATP-dependent manner. E1~Ub transfers Ub to the E2 enzyme active site cysteine in a transthiolation reaction to form E2~Ub conjugate. RING-mediated E3s mediate the transfer of Ub directly from the E2 to a substrate lysine sidechain. HECT/RBR E3s are charged with Ub at the active site cysteine in a transthiolation reaction with E2~Ub to form an E3~Ub covalent prior to Ub transfer to a substrate lysine sidechain.

The link that occurs between Ub and substrates is typically an isopeptide bond between the C-terminus of Ub and a lysine sidechain on a substrate. Because ubiquitin has lysine sidechains, it too can serve as a substrate for ubiquitin modification. Multiple rounds of the cascade result in the formation of poly-Ub chains on substrates, which give rise to distinct signaling fates depending on

type of Ub linkage on a substrate. For example, when substrates are modified by a single ubiquitin (mono-Ub), there are often changes in protein-protein interactions involving the substrate. In contrast, when substrates are modified by a poly-Ub chain linked via K48 on ubiquitin, those substrates are transported to and ultimately degraded by the proteasome. When substrates are modified by K63-linked poly-Ub chains, substrates are generally involved in DNA damage response or immune response. Mixed chains of varying Ub-Ub sidechain linkages can occur, as can branching points in which multiple lysine sidechains on a single Ub unit are modified, but these modifications are not yet well-understood. The so-called "ubiquitin code" orchestrates the complex regulation of protein homeostasis in the eukaryotic cell.

The human proteome includes 2 E1s, 40 E2s, and hundreds of E3s. Most of the specificity in the ubiquitin cascade arises from the specificity between E2s, E3s, and their substrates: E3 ligases are responsible for determining substrates, while E2s often determine the type of Ub modification (mono- versus poly-Ub) that occurs. Thus, specific E2-E3 combinations determine not only which substrates will be targeted, but how they will be targeted (Komander 2012). The type of Ub modification in turn determines the fate of the modified substrate. Numerous diseases have been linked to aberrant ubiquitin signaling, motivating decades of research into the mechanism of ubiquitin transfer at the E1, E2, and E3 levels of the cascade.

E3s are classified into three types according to three mechanisms. The most abundant class is the "really interesting new gene" or RING-type E3 class, which simultaneously bind substrate and cognate E2~Ub conjugate. By bringing substrates into proximity with E2 ubiquitin-conjugating enzymes, these E3s facilitate the direct transfer of Ub from the E2 active site cystine to the substrate lysine sidechain. In contrast, HECT- and RBR-type E3s do not necessarily simultaneously bind substrates and E2~Ubs. Instead, the E2~Ub first transfers Ub to an E3 active

site cysteine to form a covalent E3~Ub thioester intermediate, and the E3 then transfers the Ub to the substrate in a separate, additional step (Figure 1.1). RBR-type E3s are distinguished from HECT-type E3s by domains that resemble RING domains. There are roughly 30 HECT E3s, 10 RBR E3s, and over 600 RING E3s in humans (Zheng 2017).

Given the large number of E3s, the scope of the task at hand for the 40 E2s in the human proteome is a substantial one: E2s must discriminate amongst hundreds of E3s to engage their cognate E3s, thereby ensuring proper substrate ubiquitination. Understanding the rules that govern interactions between E2s and E3s, as well as E3s and their substrates, would provide an enormous benefit in understanding many pathologies that arise from aberrant ubiquitin signaling. For decades, E3 ligases were the primary subject of research in the ubiquitin field. More recently, E2 enzymes have been studied in greater detail. It has become clear that in order to fully understand E2-E3 interactions, both sides of the coin must be investigated.

1.2 E2 UBIQUITIN-CONJUGATING ENZYMES

E2s engage in two distinct reactions: transthiolation occurs when Ub is transferred from the E1 to E2, and aminolysis occurs when Ub is transferred from the E2 to substrate. In transthiolation, the thioester bond between the C-terminus of Ub and the active site cysteine on the E1 is simply exchanged for the chemically equivalent thioester bond between Ub and the E2 active site cysteine to form the thioester-linked E2~Ub conjugate. In HECT- and RBR-E3 mechanisms, an additional transthiolation reaction results in the transfer of Ub to the active site cysteine on the E3. In RING E3 mechanisms, the E2~Ub conjugate undergoes nucleophilic attack by lysine sidechains on substrates, resulting in the regeneration of free E2 and the covalent attachment of Ub to substrate lysines via a stable isopeptide linkage (denoted by the symbol "-").

All E2 ubiquitin-conjugating enzymes contain a core UBC domain, which is necessary and sufficient for catalytic activity, but many also harbor extensions or additional domains. E2s have been categorized into four general classes: class I E2s have no extensions, class II E2s have C-terminal extensions, class III E2s have N-terminal extensions, and class IV E2s have both N- and C-terminal extensions. Class I E2s contain only the UBC domain. This highly conserved domain consists of ~150 residues which fold into an oblong globular structure of 4 α-helices, a 3_{10} helix, and a four-stranded β-sheet (Figure 1.2). The N-terminal helix and two nearby loops form the binding interface for E3 enzymes, and are also involved in E1 binding. Thus, after the transthiolation reaction between E1 and E2 takes place, the E2~Ub conjugate must first dissociate from the E1 prior to binding an E3. Despite the fact that there are crystal structures of dozens of UBC domains, the exact mechanism of Ub transfer by E2 enzymes is still not completely understood: the active site lacks a general base that could deprotonate the attacking lysine sidechain in aminolysis, and no arrow-pushing mechanism for this reaction has been demonstrated. Nonetheless, there are many conserved features in the UBC domain that may shed light on the mechanism.

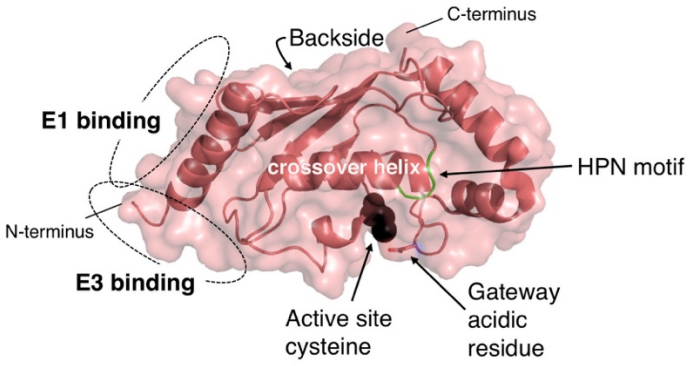

Figure 1.2. Overview of E2 UBC domain structure. Important and conserved features, motifs, and binding surfaces are depicted on Ube2D2, a class I E2 (PDB 3TGD).

In the majority of E2 UBC domains, a conserved HPN motif occurs on a loop that folds over the active site cysteine. The histidine and proline are thought to be structural, while the asparagine is thought to play a catalytic role in the aminolysis reaction (Wu 2003). Another conserved acidic residue near the entry to the catalytic cleft, termed the gateway residue, has been shown to be crucial in many E2s for aminolysis reactivity (Stewart 2016). Collectively, these active site features facilitate the formation of isopeptide bonds between Ub and substrate lysine sidechains. Another conserved feature on the UBC domain occurs on the crossover helix, which runs perpendicular to the N-terminal helix and the two C-terminal helices. There are conserved hydrophobic residues exposed on this E2 helix that have been shown to interact with a hydrophobic patch formed by I44 on the Ub surface. In the context of the covalent E2~Ub conjugate intermediate, this hydrophobic interaction enforces a closed, compact conformation which is thought to make the scissile thioester bond between Ub and the E2 active site cysteine more labile. In support of this notion, many E2 enzymes with hydrophobic crossover helix residues exhibit faster turnover rates with WT Ub than with the I44A variant of Ub, which disfavors the compact conformation (Stewart 2016).

Finally, there is another conserved feature on the UBC domain that is distant from both the active site cysteine and from the E1 and E3 binding interfaces. The “backside” surface formed by the UBC β-sheet has been shown to mediate interactions between E2s and other proteins, including noncovalently bound Ub. The role of backside binding in E2 regulation is still emerging, but it has already been shown to modulate processivity in poly-Ub chain assembly (Brzovic 2006, Middleton 2017).

The majority of E2s have other domains in addition to the UBC domain, including insertions and extensions. One example of a class II E2 (the C-terminal extension class) is Ube2K.

Ube2K's C-terminal extension folds into a distinct globular domain which associates noncovalently with Ub. The specific binding between the C-terminal domain and incoming Ub molecules is thought to enforce the construction of K48-linked polyUb chains (Middleton 2015). Ube2E1 is a class III E2 enzyme, the class of E2s with N-terminal extensions. In this case, the extension is disordered and appears to limit the assembly of polyUb chains (Schumacher 2013). The class IV E2s have both N- and C-terminal extensions, and include E2s with E3 domains on the same polypeptide chain (BIRC6), as well as E2s with smaller extensions that mediate protein-protein interactions and/or modulate the activity of the UBC domain (e.g., Ube2Z) (Schelpe 2015).

Although multiple E2s of each class have been studied in detail, we are still far from understanding all of the rules that govern the E2 structure-function paradigm. For example, the disordered extension on Cdc34 facilitates tight binding to its cognate E3 complex (Kleiger 2009), whereas in Ube2E1, the disordered extension appears to inhibit polyUb chain formation by an undefined mechanism (Schumacher 2013). There is still much to learn from studying the structure and function of other E2 extensions which will undoubtedly improve our understanding of E2 specificity in the ubiquitin cascade.

Ube2H is an example of a class II E2 ubiquitin-conjugating enzyme which possesses a UBC domain and a C-terminal extension of 32 amino acids. This thesis focuses on Ube2H as a case study in E2 extensions.

1.3 UBE2H HISTORY

Ube2H was first isolated from human placenta and subsequently cloned by Peter Kaiser et al. in 1994 following the isolation and description of the yeast homolog Ubc8 in 1991 (Kaiser 1994, Qin 1991). Ube2H shares 54% sequence similarity with the yeast ubiquitin-conjugating enzyme Ubc8, and importantly, both sequences contain long and acidic C-terminal extensions. In contrast to other

E2s that had been characterized at the time, disruption of the *ubc8* gene in yeast did not result in any obvious deleterious phenotype. Despite the lack of a known biological role, the authors nonetheless showed that the purified enzyme was capable of ubiquitinating the histone H2A/H2B dimer in the absence of an E3 ligase *in vitro*. Subsequently, Kaiser et al showed that the C-terminal extension of Ube2H was necessary for this activity. Deleting the C-terminal extension from Ube2H resulted in loss of *in vitro* H2A/H2B ubiquitylation, while cloning the extension into another E2's UBC domain (incapable of ubiquitylating H2A/H2B on its own) resulted in a gain-of-function in H2A/H2B ubiquitylation activity (Kaiser 1995). The authors concluded that the C-terminal domain of Ube2H was responsible for binding the H2A/H2B substrate, and its UBC domain was responsible for the ubiquitin-conjugating activity.

Although E3-independent substrate ubiquitylation activity is unusual for E2 enzymes (even *in vitro*), at the time of there was still no biological evidence to suggest that this function was relevant *in vivo*. To date, the biological role of Ube2H remains elusive, at least in part because there have not been extensive, targeted studies of Ube2H's function in cells or animal models. This, in turn, is likely due to the fact there have been very few reports of disease-associated mutations of Ube2H in clinical cases.

1.4 BIOLOGICAL ROLE OF UBE2H

Ube2H (also known as UbcH2, Ubc8, Gid3, and E2-20K) has been detected in both the cytosol and mitochondria, and is ubiquitously expressed in all human cells (Uhlén 2015, Thul 2017). The Ube2H sequence does not include any identifiable protein localization signals (Emanuelsson 2000). There are no reported OMIM gene-phenotype relationships in the human clinical data. High expression of Ube2H is considered an unfavorable prognosis in patients with pancreatic cancer, but the underlying mechanism behind the correlation is unknown (Uhlén 2017). The *ube2h* gene

is located on chromosome 7, and there is some preliminary evidence to suggest that it could be part of the 7q susceptibility loci for autistic disorder (Vourc'h 2003). Expression of the *ube2h* gene is regulated by the Tal1 transcription factor, which plays an important role in erythroid and hemopoietic differentiation (Lausen 2010). There is no statistically significant deleterious phenotype for Ube2H deletion in mice (Dickinson 2016), nor in the *C. elegans* ortholog Ubc-8 (Thompson 2013). However, it is possible that phenotypes for deletion in model organisms may only arise in specific conditions. Many E2s perform partially redundant functions in cells, making it challenging to parse the specific function of one E2 over another. Nonetheless, orthologs of Ube2H are present in organisms as distant from humans as nematodes, suggesting that Ube2H indeed performs some important function. In short, research into the biological function of Ube2H is in its nascent stage, and the biological function of Ube2H remains to be more fully elucidated.

1.5 COGNATE E3S OF UBE2H

Ube2H has been reported to function with many E3s *in vitro*, but in many cases there is no evidence of an *in vivo* interaction. This is because Ube2H is commercially available as a component of E2 screening kits (e.g., Boston Biochem), which are frequently used to identify uncharacterized proteins as E3 ligases and/or to identify the E2 with which those E3s function. In cases where Ube2H is the most active E2, Ube2H has been used in subsequent biochemical characterization of E3s, with the caveat that these *in vitro* results lack biological evidence to support whether the interactions are relevant *in vivo*. Nevertheless, the studies that have arisen from these screens could provide insight into the bona fide biological role of Ube2H.

1.6 TRIM28-MAGEC2 AND P53 UBIQUITYLATION

Ube2H has been reported to function with the RING E3 ligase TRIM28 and the melanoma-associated antigen MAGEC2 to ubiquitinate the tumor suppressor p53 (Doyle 2010). Prior to the 2010 Doyle publication, it was only known that TRIM28 played a role in p53 ubiquitination via an indirect mechanism. In the indirect mechanism, TRIM28 associates with MDM2 (another E3 ligase), thereby stimulating the formation of the p53-HDAC1 complex and ultimately promoting p53 ubiquitination and degradation (Wang 2005). In contrast, Doyle et al. propose that TRIM28 directly ubiquitinates p53 in the absence of MDM2. TRIM28 ligase activity toward p53 is enhanced by the presence of melanoma-associated antigen MAGEC2, which is highly expressed in many cancers. Ube2H was the only E2 enzyme capable of catalyzing TRIM28/MAGEC2-mediated p53 ubiquitination from a screen of over 10 representative E2s. Doyle et al. showed that MAGEC2 binds Ube2H *in vivo* and *in vitro* in coimmunoprecipitation assays (endogenous and epitope-tagged), and suggested that MAGEC2 may enhance TRIM28 activity by simultaneously binding Ube2H~Ub and the TRIM28-p53 complex, to effectively increase the rate of p53 ubiquitylation. The authors mapped binding between TRIM28 and MAGEC2 but did not investigate origins of specificity for Ube2H over other E2s. Overall, the results from this paper provide biochemical evidence that Ube2H may indeed function with the TRIM28-MAGEC2 ligase complex; however, in the absence of MAGEC2, it is not clear that Ube2H functions with TRIM28. Further work is needed to understand both the biological relevance and mechanistic details of the TRIM28/MAGEC2-Ube2H interaction.

1.7 MG53 AND SKELETAL MYOGENESIS

Ube2H has also been reported to function with MG53 (also known as TRIM72), a RING E3 that is muscle-specific and upregulated during skeletal myogenesis (Lee 2010, Yi 2013). In particular, Ube2H and MG53 function to ubiquitylate insulin receptor substrate-1 (IRS-1) and focal adhesion kinase (FAK), in both cases for proteasomal degradation (Lee 2010, Nguyen 2014, Yi 2013). Consequently, the authors of these papers have proposed that MG53 negatively regulates skeletal myogenesis *in vivo*, potentially with the help of Ube2H. Ube2H coimmunoprecipitates with MG53 both *in vitro* and *in vivo*, and knockdown of either Ube2H or MG53 results in a proteasome-dependent accumulation of ubiquitinated IRS-1 and FAK (Yi 2013, Nguyen 2014). Importantly, however, the biochemical activity between MG53 and Ube2H has not been reconstituted *in vitro*. It is possible that Ube2H could play an indirect role in IRS-1 and FAK ubiquitination, and that other enzymes are required for the observed activity upon Ube2H knockdown. Further research is needed to understand the role Ube2H may play in MG53-mediated IRS-1 and FAK ubiquitination.

1.8 GID COMPLEX AND GLUCONEOGENESIS

Finally, Ube2H has also recently been reported to function with the glucose-induced degradation deficient (GID) RING-E3 complex (Lampert 2018). Ube2H is the only E2 enzyme found to induce GID autoubiquitination *in vitro* out of a panel of E2s, including others E2s with acidic C-terminal extensions. The yeast homolog of the GID complex is known to function with Ubc8, the yeast homolog of Ube2H, to ubiquitylate the gluconeogenic enzyme FBPase upon a shift to glycolytic growth conditions (Schüle 2000, Santt 2008). Lampert et al. demonstrated that Ube2H is indeed the functional E2 for the human GID complex and identified novel substrates, including Hbp1, a negative regulator of pro-proliferative genes. These exciting results suggest that at least in the

context of the GID complex, Ube2H plays a role in the switch from gluconeogenesis to glycolysis. More research is needed to understand the degree to which the GID complex is specific for Ube2H as its cognate E2 and to understand the structural origins of such specificity.

Chapter 2. RESULTS AND DISCUSSION

2.1 STRUCTURE AND DISORDER

Ube2H's core UBC domain shares sequence similarity with canonical UBC domains. The Ube2D family of E2 enzymes is considered the standard against which unusual E2s are often compared. Figure 2.1 shows a sequence alignment of Ube2H's core UBC domain against the four Ube2D family member UBC domains.

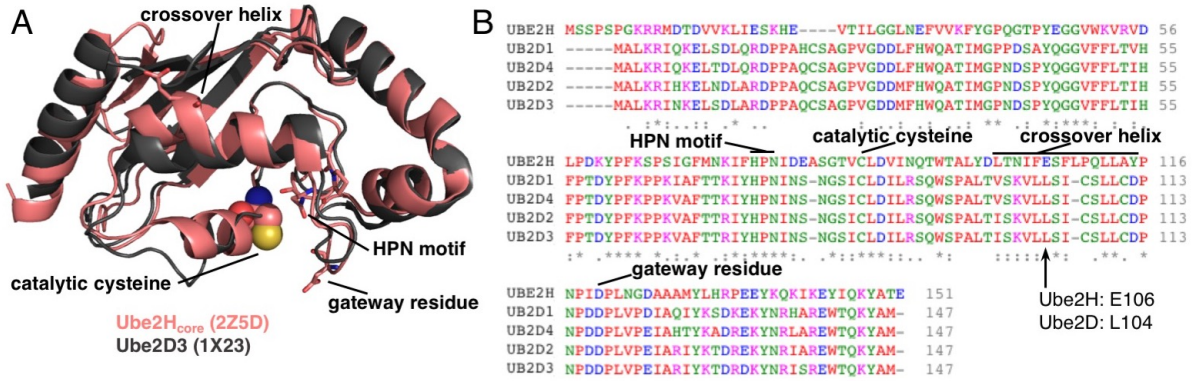

Figure 2.1. Alignment of Ube2H and Ube2D3 UBC domains. (A) Overlay of Ube2D3 (PDB 1X23) and the UBC domain of Ube2H (PDB 2Z5D) with canonical UBC features indicated. (B) Multiple sequence alignment of the human Ube2H core UBC domain (residues 1-151) against human Ube2D enzymes generated using ClustalW. Canonical UBC domain motif features are indicated.

Ube2H harbors the conserved HPN motif within its UBC domain as well as the canonical acidic gateway residue (D120). Ube2H possesses one unusual UBC domain feature: while the solvent-exposed face of the crossover helix is usually hydrophobic, Ube2H has an acidic residue exposed in the helix. In Ube2D family enzymes, L104 plays a critical role in interactions with the I44 hydrophobic patch of Ub in the thioester conjugate; in Ube2H, the acidic residue at the equivalent position (E106) suggests that the interaction may not occur in the Ube2H~Ub conjugate. The crossover helix of Ube2H also has an additional residue that results in a bulge of the crossover

helix relative to the canonical UbcH5 UBC domain, lending support to the notion that interactions with Ube2H's crossover helix may differ from those of typical E2s. To test this hypothesis, I compared the rates of aminolysis for Ube2H~Ub conjugates charged with either Ub_{WT} or Ub_{I44A}. In these assays, Ube2H was charged with either Ub variant, and lysine was added to initiate aminolysis as a proxy for a substrate lysine sidechain (Wenzel 2011).

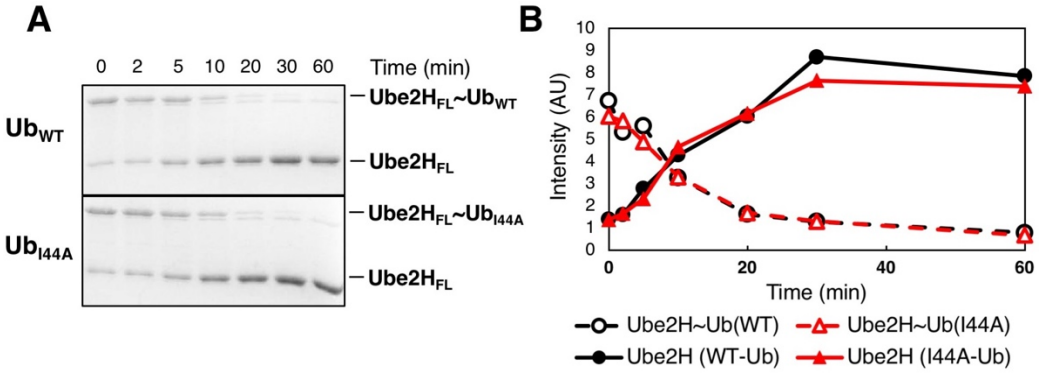

Figure 2.2. Intrinsic reactivity assay of Ube2H~Ub conjugates with UbWT or UbI44A. (A) Ube2H~Ub conjugates were formed in one-hour charging reactions with E1, Ub (WT or I44A), and $MgCl_2$/ATP, charging was quenched by EDTA, and aminolysis reactions were initiated by addition of lysine. Samples were taken at indicated timepoints, run under non-reducing conditions to preserve thioester Ube2H~Ub conjugates, and stained by Coomassie. (B) Quantification of bands in the intrinsic reactivity assay for both WT-Ub (black circles) and I44A-Ub (red triangles) conjugates quantified by both the disappearance of Ube2H~Ub (dashed lines, open symbols) and the appearance of Ube2H (solid lines, filled symbols).

The intrinsic reactivities of Ube2H~Ub conjugates were roughly equivalent whether conjugates were charged with Ub_{WT} or Ub_{I44A} (Figure 2.2). This suggests that the hydrophobic interaction between the Ub I44 hydrophobic patch and the crossover helix does not play a critical role in intrinsic Ube2H~Ub reactivity. When the same assay is performed on Ube2D family enzymes, there is a severe defect in the rate of lysine reactivity in the Ub-I44A conjugates (Mikaela Stewart, personal communication). The crystal structure of Ube2H's UBC domain shows that the

core adopts the canonical UBC domain fold (Figure 2.1), but the construct used for crystallization lacked the C-terminal extension (Sheng 2012). Secondary sequence prediction software indicates that Ube2H's C-terminal tail is likely to be disordered (Drozdetskiy 2015). To gain structural insight about the structure of full-length Ube2H, the two dimensional ^{15}N, ^{1}H- HSQC spectra were collected and compared for two Ube2H constructs: the full-length (FL) enzyme, and the Ube2H core-domain only (core). An overlay of the two spectra is shown in Figure 2.3.

The results in Figure 2.3 reveal several intriguing properties of Ube2H's structure. First, there are several UBC domain peaks that occur at different chemical shifts depending on the presence or absence of the C-terminal extension. Since the chemical shift in an HSQC experiment reports on the local chemical environment of a residue, a chemical shift perturbation (CSP) of a peak reflects a change in local chemical environment. The CSP analysis in Figure 2.3 reveals that many residues in the core domain of Ube2H are sensitive to the presence of Ube2H's C-terminal extension. The C-terminal UBC domain residues 146-151 exhibit the largest CSPs, reflecting the changes resulting from covalent addition of the C-terminal extension in the $Ube2H_{FL}$ construct. CSPs at residues distant in sequence from the C-terminal extension are more likely to be attributable to noncovalent interactions. In particular, residues 39 and 49-51 display large CSPs. These backside β-sheet residues form a surface and a groove adjacent to the C-terminal residues of the core domain, as shown in Figure 2.3C. N72 is also highly perturbed; this residue is in a backside loop that also neighbors the core domain's C-terminus. The presence of the C-terminal extension undoubtedly changes the local chemical environment of that region, explaining the high CSPs for these residues. Another highly perturbed residue is F75, which is mostly buried loop residue that neighbors the HPN motif. However, no other residues in the catalytic cleft undergo CSPs that would be consistent with a local rearrangement in that region of the core domain.

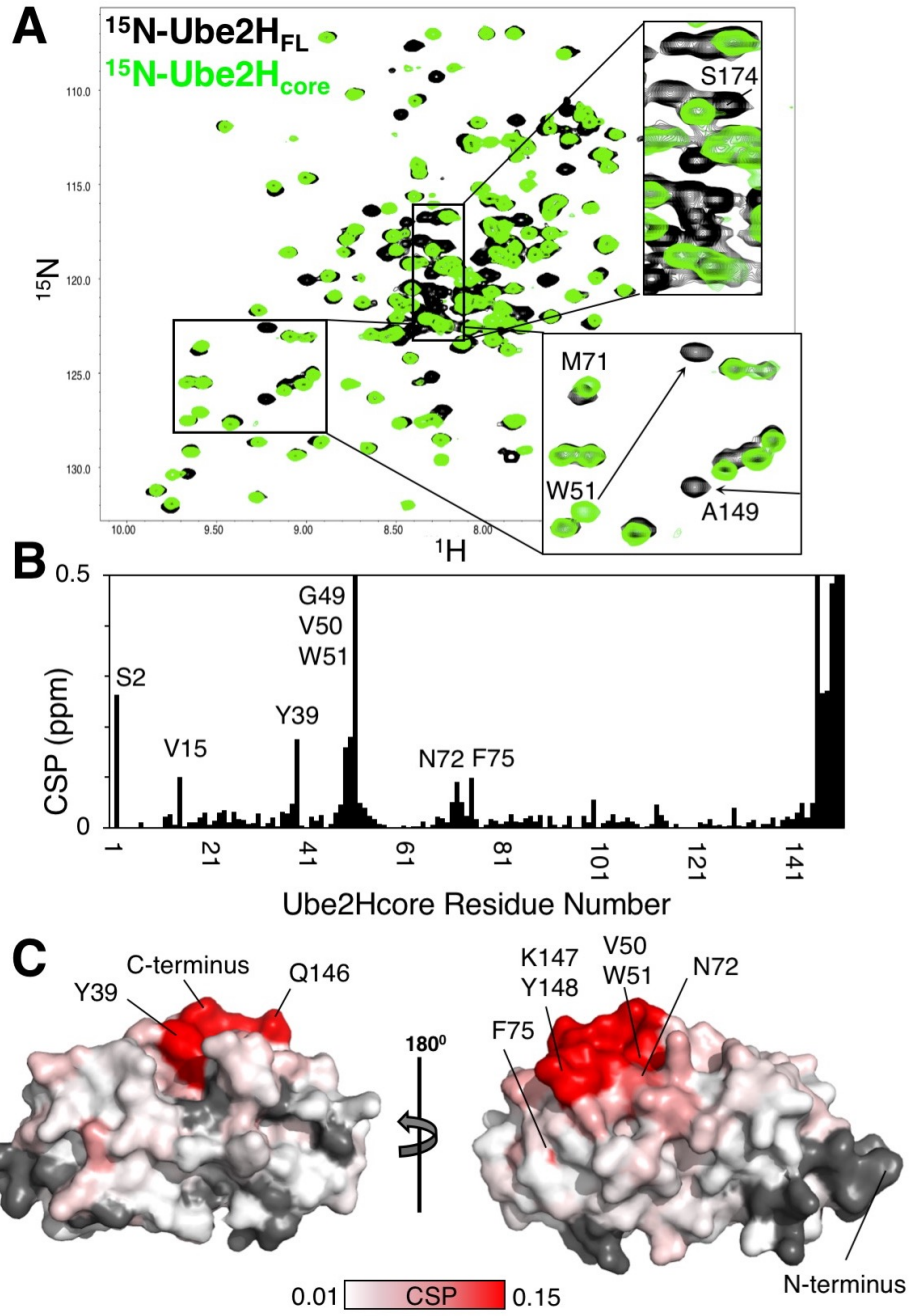

Figure 2.3. (A) Overlay of HSQC spectra of ^{15}N-Ube2H$_{FL}$ (black) and ^{15}N-Ube2H$_{core}$ (green). (B) Chemical shift perturbations (CSPs) are plotted as a function of Ube2H$_{core}$ residue number. Residues highly perturbed by the C-terminal extension are indicated. Unassigned Ube2H$_{core}$ residues are shown as blanks. (C) CSPs mapped onto the Ube2H$_{core}$ crystal structure (PDB 2Z5D) according to the indicated scale. Unassigned Ube2H$_{core}$ residues are shown in grey. Left: Ube2H$_{core}$ shown with the crossover helix facing out as in Figure 2.1A; Right, Ube2H$_{core}$ shown with the back surface facing out.

The N-terminal domain residue S2 undergoes a large CSP, indicating that the C-terminal extension may interact with the N-terminal region. S2 is in a short four-residue disordered region before the N-terminal helix (no density in the crystal structure), and is the only residue with an assigned HSQC peak. If an interaction with these disordered N-terminal residues (M1-P4) occurred, there would likely be CSPs on nearby residues as well, but poor coverage in neighboring residues prohibits any strong conclusions about the potential interaction. The N-terminal helix includes 17 residues (S5-S21) of which D12-S21 are all assigned (Figure 2.3B). V15 has a large CSP, while the other assigned N-terminal helix residues do not. V15 is buried and is therefore unlikely to directly interact with the C-terminal extension (it may instead be allosterically perturbed). Due to the poor coverage for N-terminal residues, it is not possible to conclude whether the C-terminal extension interacts in cis with the N-terminal side of the N-terminal helix. Nonetheless, the fact that two residues in the N-terminal domain are among the most highly perturbed $Ube2H_{core}$ residues when the C-terminal extension is present lends support to the possibility that in $Ube2H_{FL}$, the C-terminal extension may contact the N-terminal helix. The N-terminal helix is known to be involved in E1 (and to some extent E3) interactions (see Figure 1.2), so an interaction between the C-terminal extension and this UBC domain region could in principle affect interactions with E1 and E3 enzymes.

Importantly, the core domains of some other E2s with disordered extensions do not undergo chemical shift perturbations in the presence of their respective extensions. Ube2T, for example, has a disordered C-terminal extension of 40 residues, but no core domain residues exhibit chemical shift perturbations in an overlay of its FL and core domain HSQC spectra (Mikaela Stewart, unpublished results). For Ube2H, the UBC domain CSPs that occur in the presence of the C-terminal extension are consistent with at least two possibilities: the extension may allosterically

alter certain UBC domain residues, or the extension may directly contact a subset of core domain residues. The data in Figure 2.3 do not discriminate between these two possibilities, and further structural techniques will be needed to understand the mechanism by which the UBC domain of Ube2H is perturbed by the presence of the C-terminal extension.

In addition to potential interactions between Ube2H's C-terminal extension and UBC domain, the data in Figure 2.3 also provide insight into the structural state of the C-terminal extension in $Ube2H_{FL}$. Many of the C-terminal extension peaks in the $Ube2H_{FL}$ spectrum are strong and occur in the random coil region (see S174 region in Figure 2.3A), consistent with properties of disordered residues. Secondary sequence propensity was calculated for each C-terminal extension residue using the chemical shifts for backbone C_α and C_β atoms (Figure 2.4). Indeed, residues G160-L183 have propensities consistent with intrinsically disordered proteins (near zero), while E151-E156 have propensities toward α-helical structure. Ube2H's C-terminal extension appears to be mostly disordered, as predicted.

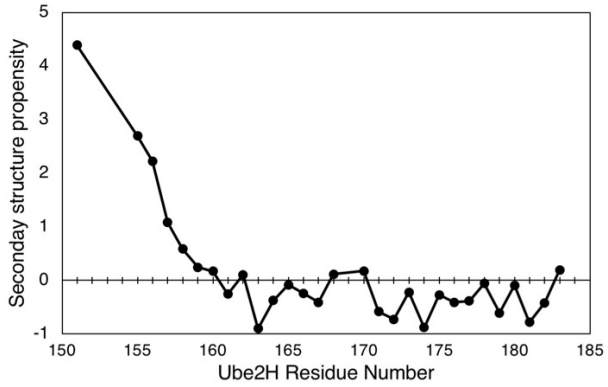

Figure 2.4. Secondary structure propensity plotted as a function of Ube2H C-terminal extension residue number.

2.2 PHYLOGENETIC CONSERVATION

Orthologs of Ube2H occur in organisms as distant as nematodes, yeast, and slime molds. To gain insight into the possible structural and functional significance of Ube2H's C-terminal extension, the primary sequences of Ube2H orthologs were analyzed for phylogenetic conservation. Excluding partial sequences and sequences from uncultured/environmental samples, every Ube2H homolog contains a C-terminal extension. Moreover, there are conserved features within the C-terminal extension. Figure 2.5 shows conservation scores calculated by the bioinformatics software ConSurf (Ashkenazy 2016) onto a model of $Ube2H_{FL}$ generated using MODELLER (Webb 2016). The phylogenetic analysis reveals that in general, residues the core UBC domain of Ube2H are more highly conserved than in the C-terminal extension. Interestingly, the final helix of the UBC domain preceding the C-terminal extension is less conserved than other regions of the UBC domain. The final two UBC domain helices of E2 enzymes are not often involved in E1 or E3 binding, which could explain the reduced conservation in that region of Ube2H.

Notably, although Ube2H's C-terminal extension is not strongly conserved at the residue-specific level, all orthologs found in the UniProt database contain the long C-terminal extension domain, ranging from 32 residues in humans to 69 residues to the yeast homolog Ubc-8. These C-terminal extensions vary in length, yet intriguingly, each extension is both serine-rich and acidic. Moreover, there is a highly conserved MEL motif in the final C-terminal residues; this motif has not been reported in other proteins. ConSurf predicts two of the C-terminal domain serines and the MEL motif to be functional due to their surface exposure and high conservation. The fact that all Ube2H orthologs have C-terminal extensions which harbor conserved features strongly suggests that there is some important role for the C-terminal extension in Ube2H's biological function.

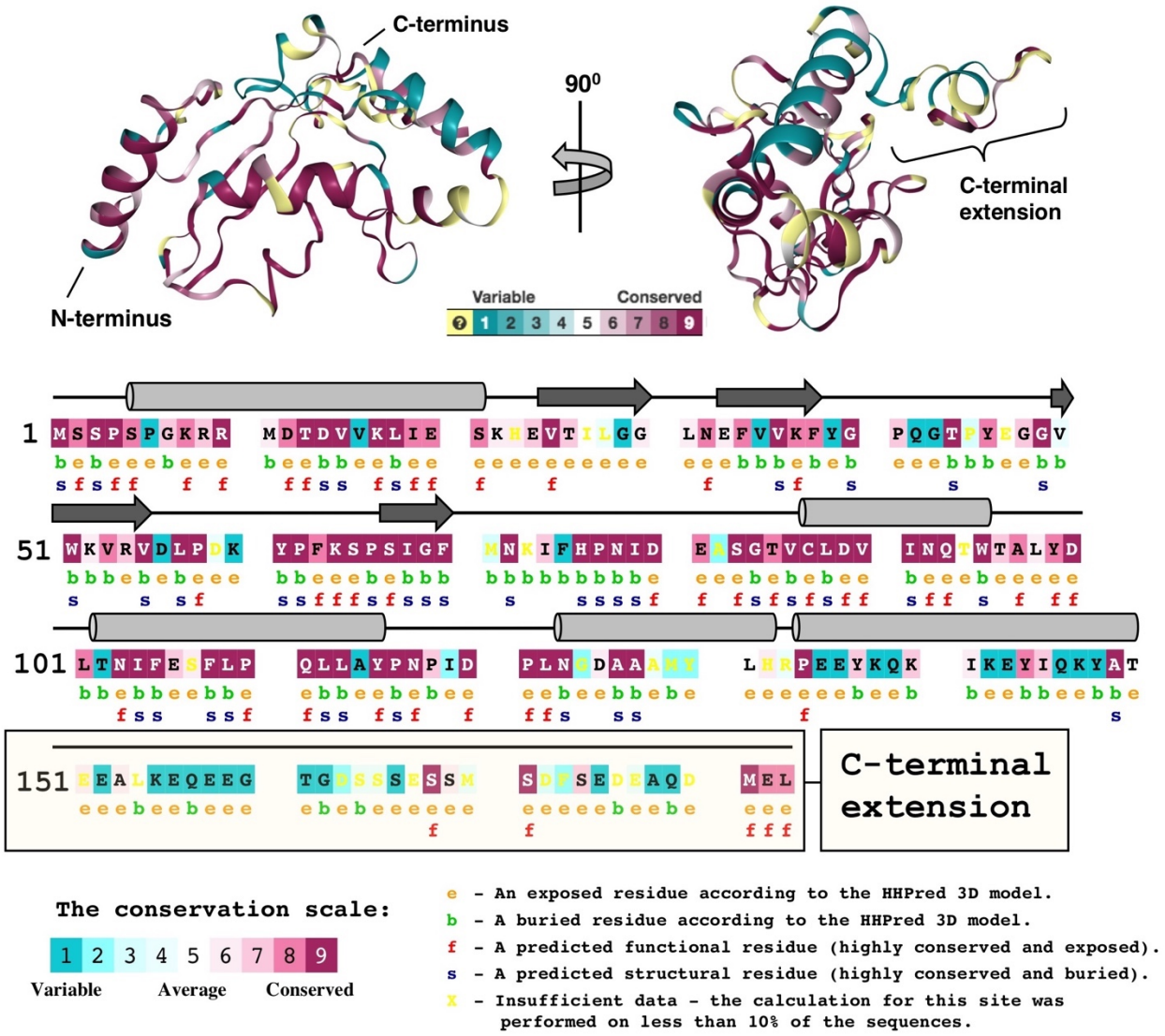

Figure 2.5. Phylogenetic conservation scores mapped onto a model of $Ube2H_{FL}$. Conservation scores were calculated using ConSurf based on orthologs in the UniProt database aligned using MAFFT. Above, conservation scores are mapped by color onto a model of $Ube2H_{FL}$ built using MODELLER. Below, conservation scores are mapped by color onto the human Ube2H primary sequence with secondary sequence features indicated.

2.3 POSSIBLE POST-TRANSLATIONAL MODIFICATIONS

Disordered and serine-rich extensions are often targets for phosphorylation, and the conservation analysis shown in Figure 2.5 predicts that the C-terminal extension residue serine S171 may be functional due to its solvent exposure and high conservation. Phosphosite prediction software (NetPhos3.1, NetPhorest) predicts that all seven serines in Ube2H's C-terminal extension have high potential for phosphorylation (Blom 1999, Miller 2008). To determine whether S171 or other residues could be subject to post-translational modifications (PTMs), I consulted phosphorylation databases for Ube2H-specific data. Database searches for evidence of *in vivo* phosphorylation did not yield any results indicating any PTMs in Ube2H's C-terminal extension (PhosphoSitePlus, Hornbeck 2015). However, the absence of PTM data on Ube2H's extension could be attributable to coverage limitations, since Ube2H lacks trypsin cleavage sites in its C-terminal domain that would yield sufficiently small, MS-detectable peptide fragments. Alternative proteases could cleave the Ube2H C-terminus and yield peptides that would reveal the PTM-state of the extension *in vivo*. Phosphosite databases are largely populated by high-throughput MS screens, and a more targeted approach would be necessary to determine whether PTMs occur on Ube2H's C-terminal extension in cells. Nonetheless, there is considerable evidence that Ube2H is phosphorylated at an N-terminal residue (S3) (Minard 2016, Malec 2015, Pinto 2015, Verano-Braga 2012, Gauci 2009) and ubiquitylated at a site adjacent to the N-terminal helix (K60) (Akimov 2018, Wagner 2012, Povlsen 2012, Wagner 2011). Both of these sites are highly conserved (Figure 2.5). Though the phosphosite data derived from high-throughput techniques must be validated, it is an intriguing possibility that Ube2H could be regulated by one or more of these post-translational modifications.

2.4 UBIQUITYLATION ASSAYS

With the insight that Ube2H's C-terminal extension is conserved, I aimed to search for a functional purpose of the extension with respect to enzyme activity. Since E2 enzymes are the intermediate enzymes of the ubiquitylation cascade, the C-terminal extension could in principle alter one or more steps in the cascade. E2 enzymes participate in transthiolation reactions with E1~Ub to form E2~Ub (in HECT- and RBR-E3s, E2~Ub conjugates carry out a second round of transthiolation to form E3~Ub) and also participate in aminolysis reactions with substrate lysine sidechains. In both types of reaction mechanisms, the C-terminal extension could play a direct role by interacting with E1, E3, or substrate, or an indirect role by allosterically modulating the reactivity of the E2. Ubiquitylation assays were carried out using recombinantly purified enzymes *in vitro* to examine the functional effects of deleting Ube2H's C-terminal extension.

I first tested whether reactivity between Ube2H and human E1 (Uba1) enzyme varied depending on the presence of Ube2H's C-terminal extension. Two Ube2H constructs ($Ube2H_{FL}$ or $Ube2H_{core}$) were combined with Ub, E1, and MgCl2/ATP, and reactions were monitored for the appearance of products. For both Ube2H constructs, the products included thioester-linked Ube2H~Ub, autoubiquitylated isopeptide-linked Ube2H-Ub_n, and polyUb chains (Figure 2.6).

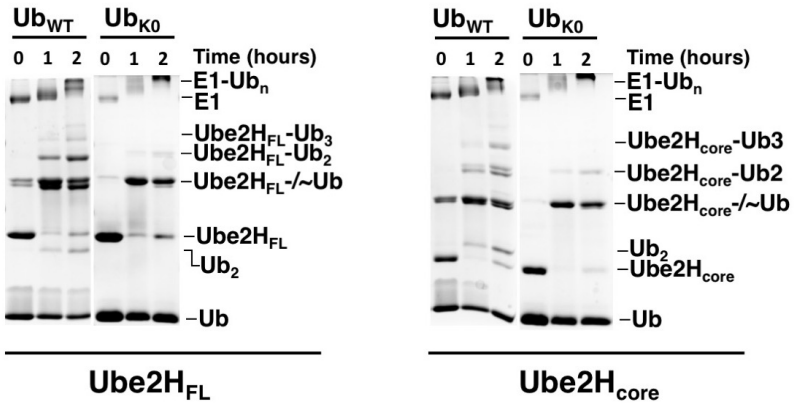

Figure 2.6. Ube2H autoubiquitylation and polyUb chain-building assay with $Ube2H_{FL}$ and $Ube2H_{core}$. Samples were taken at indicated timepoints, run under non-reducing conditions to preserve thioester Ube2H~Ub conjugates, and stained by Coomassie. Reactions with WT-Ub reveal multiple higher molecular weight bands which were further probed in reactions with K0-Ub, a variant of Ub which is incompatible with polyUb chain formation. Ube2H~/-Ub denotes a mixed population of thioester and isopeptide-linked Ube2H~Ub and Ube2H-Ub, respectively.

A qualitative comparison of $Ube2H_{FL}$ and $Ube2H_{core}$ reactivity against WT-Ub in Figure 2.6 reveals that both constructs yield similar products in the absence of an E3 and substrate. Both $Ube2H_{FL}$ and $Ube2H_{core}$ reactions yield diUb (Ub_2). For a chain-building E2 enzyme, longer polyUb chains would be expected to form under these conditions. Thus, Ube2H does not appear to possess chain-building activity regardless of the presence of its C-terminal extension. Instead, the primary products for both $Ube2H_{FL}$ and $Ube2H_{core}$ are autoubiquitylated, isopeptide-linked forms of Ube2H, including bands corresponding to single and multiple Ub modifications. A reducing gel was run on the 2-hour reaction mixture to confirm that both thioester-linked and isopeptide Ube2H~Ub/Ube2H-Ub species were present (results not shown). To differentiate between polyUb chains attached to a single lysine residue on Ube2H (polyubiquitylated) versus monoUb attached to multiple lysine residues (multi-monoubiquitylated) on Ube2H, I repeated the assay using a variant of ubiquitin in which all lysines are mutated to arginines (K0-Ub) such that

poly-Ub chain synthesis is prevented (K0-Ub cannot serve as a ubiquitylation substrate). For both Ube2H$_{FL}$ and Ube2H$_{core}$, K0-Ub results in fewer products as compared to WT-Ub. As expected, no Ub_2 is formed for either Ube2H variant. Additionally, for both variants, there are fewer bands of autoubiquitylated Ube2H, with no Ube2H-Ub_3 formed, and less Ube2H-Ub_2 formed than with WT-Ub. Comparing the assay results between WT-Ub and K0-Ub reveals that Ube2H$_{FL}$ and Ube2H$_{core}$ have a modest ability to produce unanchored Ub_2 as well as di- and tri-Ub chains anchored to Ube2H itself. It is worth noting that the conditions of this assay are far from physiological. Nonetheless, under these conditions both Ube2H$_{FL}$ and Ube2H$_{core}$ are capable of auto-monoubiquitylation, multi-monoubiquitylation, and polyubiquitylation. However, the C-terminal extension does not appear to affect any of these activities under the assay conditions tested.

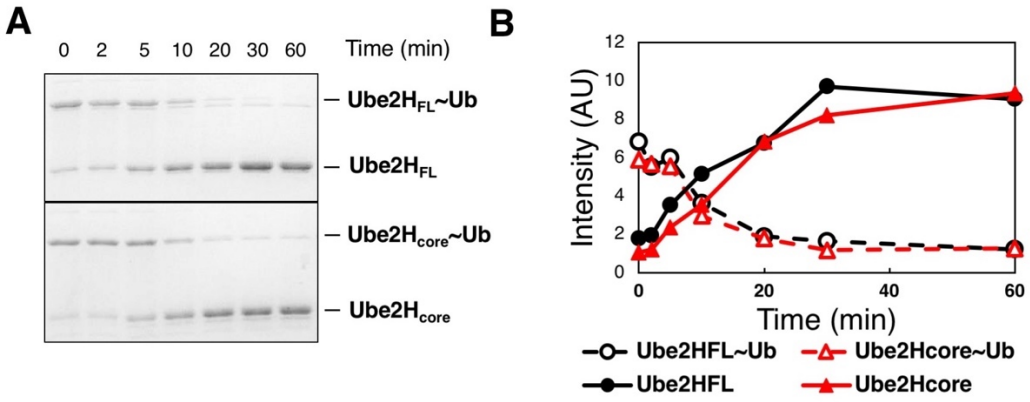

Figure 2.7. Intrinsic reactivity assay of Ube2H~Ub conjugates charged with either Ube2H$_{FL}$ or Ube2H$_{core}$. (A) Ube2H~Ub conjugates were formed in one-hour charging reactions with E1, Ub, and $MgCl_2$/ATP, charging was quenched by EDTA, and aminolysis reactions were initiated by addition of lysine. Samples were taken at indicated timepoints, run under non-reducing conditions to preserve thioester Ube2H~Ub conjugates, and stained by Coomassie. (B) Quantification of bands in the intrinsic reactivity assay for both Ube2H$_{FL}$ (black circles) and Ube2H$_{core}$ (red triangles) quantified by both the disappearance of Ube2H~Ub conjugates (dashed lines, open symbols) and the appearance of Ube2H (solid lines, filled symbols).

To test Ube2H's reactivity in aminolysis reactions, I performed intrinsic reactivity assays using free lysine as a proxy substrate in order to assess Ube2H's intrinsic activity both in the presence and absence of its C-terminal domain. Ube2H~Ub conjugates appear to be equally reactive to lysine regardless of the presence of the C-terminal domain under the assay conditions tested (Figure 2.7). Deletion of the C-terminal extension from Ube2H did not appear to hinder or enhance the rate of Ub transfer.

The C-terminal extension may affect the activity of the enzyme in the context of its cognate E3 ligase(s) and substrate(s) by directly mediating binding interactions involving Ube2H. Without a bona fide E3 ligase or substrate, I turned to histone H2B as a proxy substrate that likely mimics physiological substrates more accurately than high concentrations of free lysine in solution (H2B is used in lower concentrations than free lysine and is a globular lysine-rich protein). Ube2H was originally noted for its ability to ubiquitylate the H2A/H2B dimer in the absence of an E3 (Kaiser 1994).

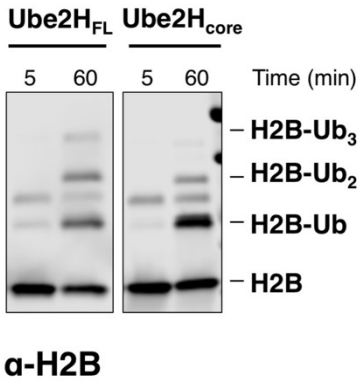

Figure 2.8. Histone H2B ubiquitylation assay in the presence of either Ube2H$_{FL}$ or Ube2H$_{core}$. E1, Ub, Ube2H (FL or core), H2B, and $MgCl_2$/ATP were combined in reaction mixtures. Samples were taken at indicated timepoints, run under reducing conditions, and visualized by anti-H2B Western blot.

The histone H2B ubiquitylation assay results in Figure 2.8 reveal an interesting difference between Ube2H$_{FL}$ and Ube2H$_{core}$ activities. Both Ube2H variants are capable of ubiquitylating H2B, but the ratio of mono- versus di- and tri-ubiquitylated H2B differs depending on Ube2H's C-terminal extension. Ube2H$_{FL}$ produces a greater proportion of di-, and tri-ubiquitylated H2B, whereas Ube2H$_{core}$ produces a greater proportion of monoubiquitylated H2B. The difference in H2B ubiquitylation products could indicate a difference in affinity for the monoubiquitylated H2B as a substrate for further modification. In particular, if Ube2H$_{FL}$ has a higher affinity for H2B-Ub and/or H2B-Ub$_2$ than Ube2H$_{core}$, then a greater number of H2B-Ub and/or H2B-Ub$_2$ will be further ubiquitylated by Ube2H$_{FL}$ than Ube2H$_{core}$.

The acidic nature of Ube2H's C-terminal extension might confer Ube2H$_{FL}$ a higher affinity for the highly basic H2B monomer than Ube2H$_{core}$, enabling it to transfer Ub to mono- and di-ubiquitylated H2B with greater frequency than Ube2H$_{core}$ construct. Interestingly, Kaiser et al. suggested that the C-terminal extension is necessary for histone ubiquitylation in the case of the H2A/H2B dimer (Kaiser 1995). The results in Figure 2.8 demonstrate that Ube2H$_{core}$ is indeed capable of ubiquitylating the H2B monomer. The disparity in these results may arise from differences in the *in vitro* assay conditions and/or substrates, but it is clear that at least under the assay conditions tested, the C-terminal extension is not strictly required for Ube2H-mediated H2B ubiquitylation.

2.5 Dynamics of Ube2H~Ub

It is estimated that the majority of E2 enzymes in cells exist in the E2~Ub conjugate form rather than in the unconjugated form. For this reason, and in light of the fact that E3 ligases must bind the E2~Ub conjugate rather than free E2 for productive reactivity, the E2~Ub conjugate is considered a more mechanistically relevant molecule to study than free E2 enzyme. In the case of

Ube2H, I considered the possibility that the C-terminal extension may affect the conformation of Ube2H~Ub conjugate. An altered conformational state could lead to enhanced binding with cognate E3 ligases, or could alter the reactivity of Ube2H~Ub. In particular, a closed conformational state of Ube2H~Ub would be predicted to lead to higher rates of aminolysis in lysine reactivity assays. Given the fact that Ube2H lacks a conserved hydrophobic residue in the crossover helix which interacts with Ub to form a closed E2~Ub conjugate state, I wondered whether the C-terminal tail could serve a compensatory role to enforce a closed Ube2H~Ub conformation. Although the data in intrinsic reactivity assays (Figure 2.7) did not reveal significant differences between the reactivities of $Ube2H_{FL}$~Ub and $Ube2H_{core}$~Ub, the results are only conclusive for the assay conditions tested.

To compare the structural features of Ube2H~Ub conjugates both with and without the C-terminal extension, I used small-angle X-ray scattering (SAXS) and NMR. For both structural approaches, I used stable oxyester mimics of both $Ube2H_{FL}$~Ub and $Ube2H_{core}$~Ub conjugates generated by mutating the E2 active site cysteine to serine (thioester-linked conjugates are reactive and hydrolyze within hours of formation). SAXS scattering profiles were collected for both $Ube2H_{FL}$-O-Ub and $Ube2H_{core}$-O-Ub oxyester conjugates. In parallel, I used MODELLER to build models of Ube2H~Ub conjugates and FoXS to generate theoretical SAXS scattering curves for each model (Schneidman-Duhovny 2016). Models were scored against averaged experimental data and the top-fitting models were compared to experimental data (Figure 2.9).

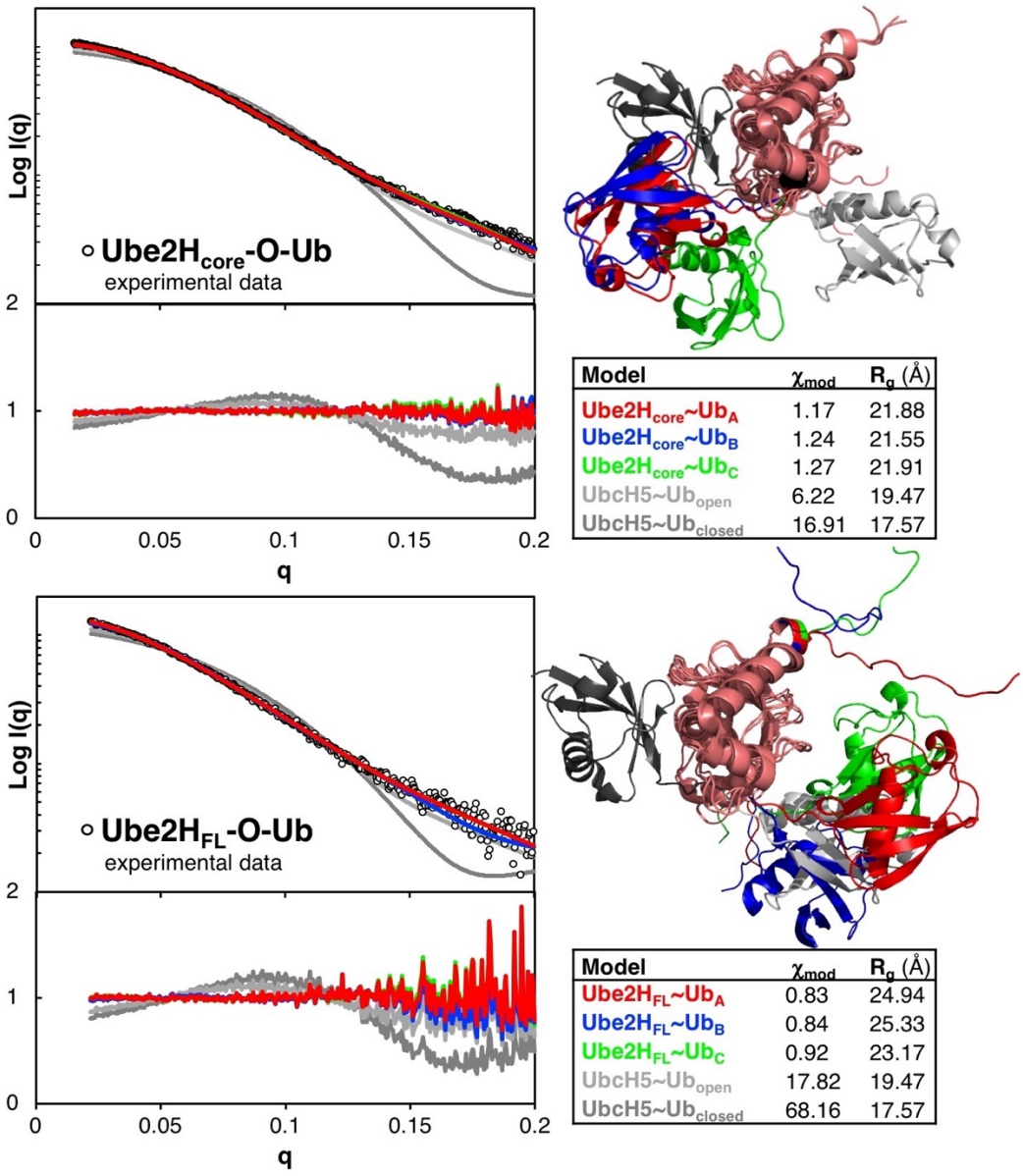

Figure 2.9. SAXS scattering curves for oxyester mimics of Ube2H~Ub conjugates and top-fitting theoretical models. Top: Ube2H$_{core}$-O-Ub, Bottom: Ube2H$_{FL}$-O-Ub. Left: experimental SAXS scattering curves are shown in hollow black circles. The theoretical SAXS curves for best-fitting models (A-C) are shown in red (best fitting), blue (second-best fitting), and green (third-best fitting). Theoretical curves generated from structures of UbcH5~Ub in an open (light gray) and closed (dark gray) are shown for comparison (PDB 3A33, 4AUQ, respectively). Lower plots show residuals from experimental data. Right: the structures of all models were aligned by the UBC domain with the Ub unit colored as in the SAXS curves. E2~Ub conjugates are shown from the side-on view. χ_{mod} and Guinier radius values for models are shown in the table.

The UBC and Ub domains are locally rigid and globular but are connected by the flexible linker formed by the thioester bond between the UBC active site cysteine and the C-terminus of Ub. Models of both Ube2H$_{core}$~Ub and Ube2H$_{FL}$~Ub exhibit a distribution of Ub positions relative to the UBC domain, but the Ube2H$_{core}$~Ub models more closely resemble a closed E2~Ub conjugate conformation than Ube2H$_{FL}$~Ub models. When compared to theoretical SAXS curves generated from closed and open structures of UbcH5~Ub, Ube2H$_{core}$-O-Ub data are more consistent with a closed conformation, while Ube2H$_{FL}$-O-Ub data are more consistent with an open conformation. In Ube2H$_{FL}$~Ub models, the C-terminal extension adopts a range of positions relative to the UBC domain, as expected for a disordered extension.

It is important to interpret these models cautiously. SAXS data measure an ensemble of conformations, and all E2~Ub conjugates are flexible multidomain proteins that adopt a continuum of conformations. For example, even E2~Ub conjugates that are considered "closed" in fact sample open-state conformations as well, but spend less time in those conformations as compared to "open" E2~Ub conjugates, and vice versa. Thus, small changes in the population distribution of E2~Ub conjugate conformational states (which could be mechanistically important) may not be detectable in low-resolution SAXS data. The models presented here are useful in guiding future structural studies and generating hypotheses to further corroborate. In particular, the SAXS-generated models in Figure 2.8 point toward a potential extension-dependent difference in the conformational ensembles of the Ube2H~Ub conjugate.

To further probe Ube2H~Ub conjugate conformational distributions, I compared the chemical shifts of Ub residues in the apo state to the state in Ube2H~Ub conjugates. I mapped the chemical shift perturbations that occur on Ub residues upon conjugation (via stable oxyester linkage) to either Ube2H$_{core}$ or Ube2H$_{FL}$ (Figure 2.10).

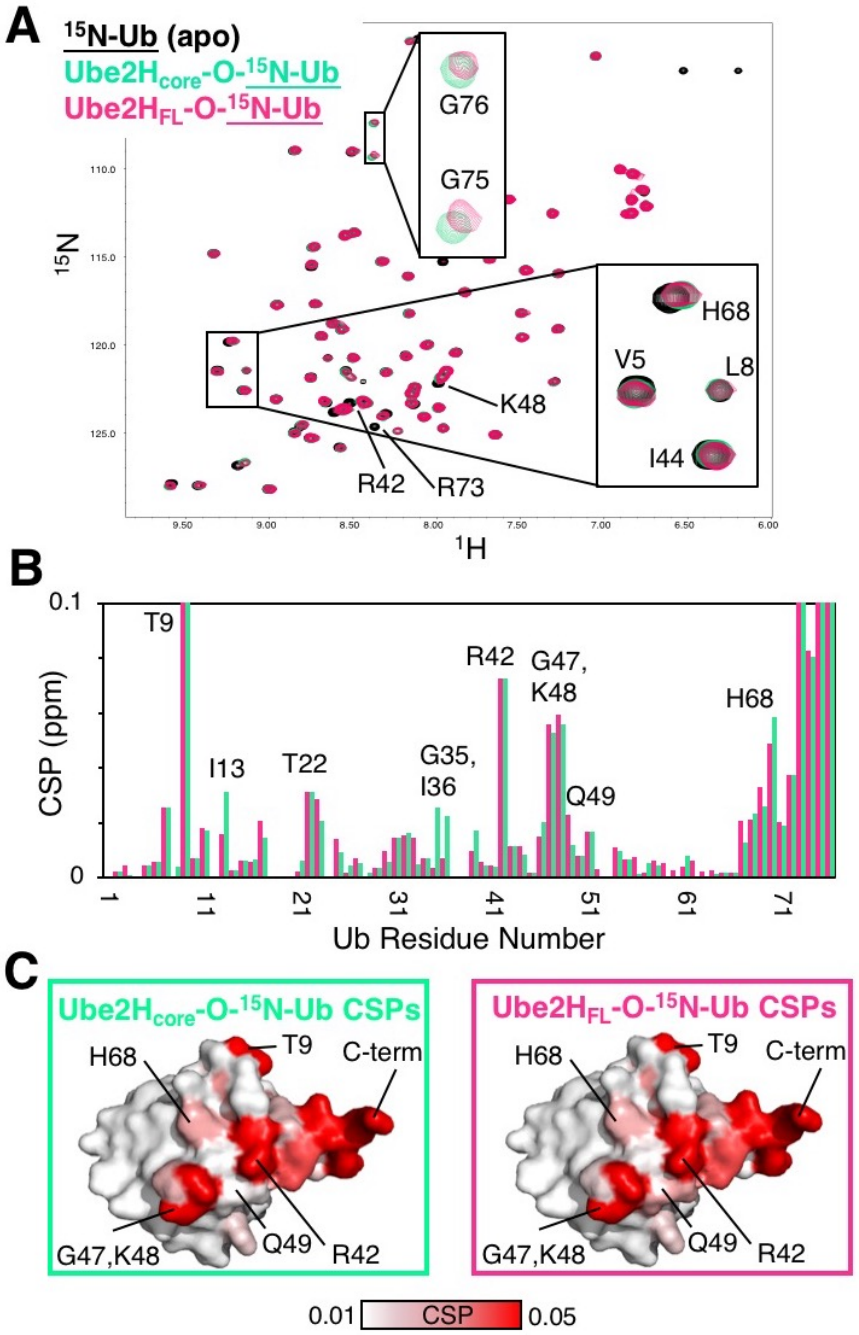

Figure 2.10. (A) Overlay of HSQC spectra of apo ^{15}N-Ub (black) and ^{15}N-Ub when conjugated via oxyester linkage to either Ube2H$_{core}$ (teal) or Ube2H$_{FL}$ (magenta). (B) Chemical shift perturbations (CSPs) plotted as a function of Ub residue number. Residues with high CSPs are indicated. Unassigned Ub residues are shown as blanks. (C) CSPs mapped onto the Ub crystal structure (PDB 1UBQ) according to the indicated scale. Unassigned residues are shown in grey.

For both Ube2H$_{core}$~Ub or Ube2H$_{FL}$~Ub, the C-terminal residues on Ub are the most affected residues after conjugation. These residues undergo covalent modification upon conjugation, so large CSPs in that region are expected, but are not informative about noncovalent intramolecular interactions between the Ub and Ube2H moieties in the conjugates. The Ub residues distant from the C-terminus that exhibit pronounced CSPs are very similar regardless of which Ube2H construct is conjugated (Figure 2.10B-C). In both cases, T9, T22, R42, G47, K48, and H68 are the residues with the largest CSPs. Of these residues, R42, G47, K48, and H68 form a surface surrounding the I44 hydrophobic patch on Ub. In Figure 2.2, both Ube2H$_{FL}$~Ub and Ube2H$_{core}$~Ub are equally reactive to WT or I44A-Ub, and these results are consistent with fact that the I44 Ub peak does not exhibit CSPs upon conjugation to either construct (Figure 2.10). The fact that the same Ub residues exhibit very similar CSPs in Ube2H$_{FL}$~Ub and Ube2H$_{core}$~Ub suggests that Ube2H's C-terminal extension does not alter Ub interactions in the conjugate, and this is consistent with the similar rates of lysine reactivity shown in Figure 2.2. Minor differences in Ub CSPs between the two Ube2H constructs occur in residues G35-I36 and Q49. The CSPs for G35-I36 and I13 are larger in the context of Ube2H$_{core}$~Ub than Ube2H$_{FL}$~Ub, while the reverse is true for Q49. To be confirmed, these CSP differences would need to be shown to be reproducible and larger than the digital resolution of the experiment. There may indeed be subtle differences in the chemical environment of Ub in the two conjugates forms. However, the similar rates of lysine reactivity suggest that even if there are differences in the conjugates, they are not mechanistically important with respect to intrinsic activity towards lysine.

The conformational differences in the Ube2H~Ub conjugate SAXS models and the Ub CSP mapping results are in mutual agreement. Figure 2.11 shows the chemical shift perturbations in Figure 2.10 mapped onto the top ten-fitting SAXS models from Figure 2.9. In both cases, the

perturbed surfaces on Ub are positioned closest to the UBC domain, consistent with similar sampling of conformational states in both Ube2H~Ub conjugates. The CSP mapping data do not lend evidence to support the notion that Ube2H$_{FL}$~Ub is in a more open state than Ube2H$_{core}$~Ub, though the changes may be too subtle to detect in the CSP-mapping experiments. For example, it is possible that similar Ub surfaces are perturbed in both cases, but the dynamics of conformational sampling are altered by the presence of the extension. Further experiments are needed to test differences in dynamics between Ube2H$_{FL}$~Ub and Ube2H$_{core}$~Ub.

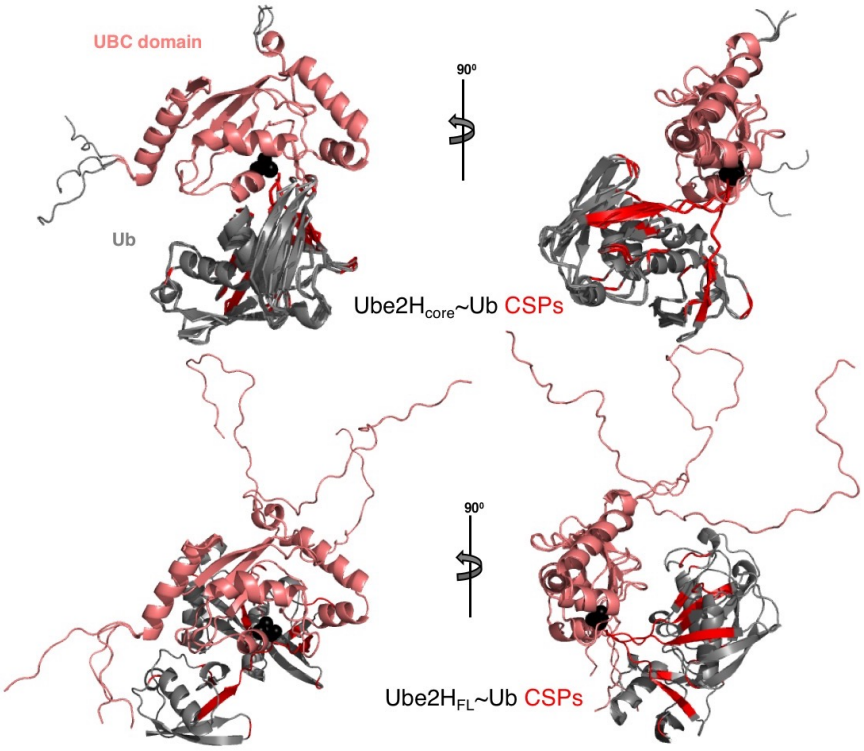

Figure 2.11. NMR chemical shift perturbations mapped onto the top-three fitting SAXS-derived models of Ube2H$_{core}$~Ub (top) and Ube2H$_{FL}$~Ub (bottom) conjugates. Ube2H is shown in salmon, Ub is shown in gray, and models are aligned by UBC domains (left structures are shown as in Figure 2.1). Ub residues with high CSPs upon conjugation are shown in red.

2.6 SEARCHING FOR AN E3 LIGASE

Structural characterization of Ube2H alone suggests that Ube2H's C-terminal extension is disordered, but perturbs residues in the UBC core domain either allosterically or through direct but transient interactions (Figure 2.3). The conformational ensembles of Ube2H~Ub conjugate models derived from SAXS data suggest that $Ube2H_{FL}$~Ub conjugates may adopt a more open state than $Ube2H_{core}$~Ub (Figure 2.9), but there are very few differences in the perturbed surfaces of Ub upon conjugation to the two Ube2H constructs (Figures 2.10). In functional assays, $Ube2H_{FL}$ and $Ube2H_{core}$ are similarly reactive (Figure 2.6-2.8). Qualitative differences in histone H2B ubiquitylation hint at a possible C-terminal extension-dependent difference in reactivity, but no such difference in reactivity is detectable with free lysine in intrinsic reactivity assays. Moreover, the differences in H2B reactivity could be attributable to simple electrostatic interactions between Ube2H's acidic C-terminal extension and the highly basic H2B monomer. My initial efforts to elucidate the function of Ube2H's C-terminal extension by considering its structural features in isolation and its reactivity with generic lysine nucleophiles failed to identify a smoking gun. Next, I considered the possibility that Ube2H's C-terminal extension may not alter the UBC domain's intrinsic activity at all, but could instead serve to enhance Ube2H's affinity for a cognate E3. Several E3s have been suggested to function with Ube2H, as discussed in Chapter 1, but neither cognate E3s nor substrates have been rigorously established. I aimed to identify a functional E3 ligase to test the hypothesis that Ube2H's C-terminal tail may be important for cognate E3 binding.

2.7 MG53/TRIM72

There are multiple reports that the TRIM E3 ligase MG53/TRIM72 functions with Ube2H to ubiquitylate the substrates insulin receptor substrate (IRS-1) and focal adhesion kinase (FAK). I

purified two truncated constructs of MG53, one containing only the catalytic RING E3 ligase domain ($MG53_{RING}$), and one including the RING domain, a small C-terminal zinc-finer domain (B-box domain), and a coiled-coil domain ($MG53_{RBCC}$). $MG53_{WT}$ includes an additional C-terminal domain of 250 residues classified as a SPla RYanodine receptor domain (SPRY domain) which may be involved in E3-substrate interactions, but is not thought to be necessary for enzymatic activity (Yi 2013, Nguyen 2014). I tested the activity of Ube2H with MG53 constructs by monitoring the rate of Ub transfer from Ube2H~Ub to free lysine in solution for both $Ube2H_{FL}$ and $Ube2H_{core}$ with both constructs of MG53 as compared to a no E3 control (Figure 2.12).

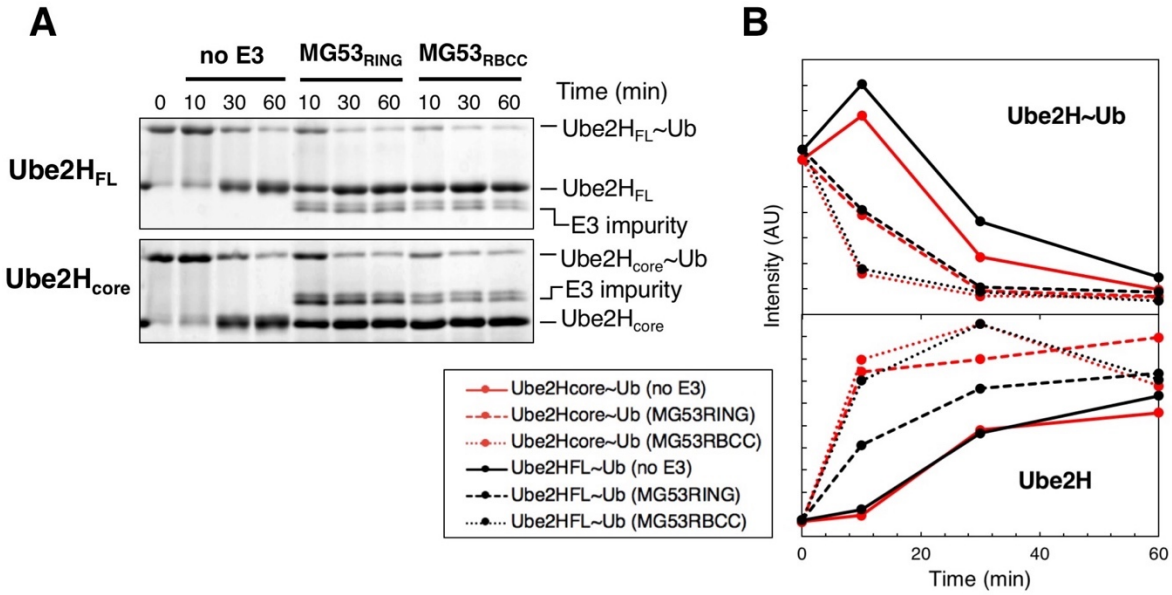

Figure 2.12. Intrinsic reactivity of Ube2H~Ub conjugates in the absence and presence of MG53. (A) Assay results for $Ube2H_{FL}$~Ub (top) and $Ube2H_{core}$~Ub (bottom) conjugates in the absence (left) and presence of $MG53_{RING}$ (middle) and $MG53_{RBCC}$ (right). (B) Quantification of bands from (A), with Ube2H~Ub shown on top and Ube2H alone on bottom. $Ube2H_{core}$ data is shown in red, and $Ube2H_{FL}$ is shown in black.

For both $Ube2H_{FL}$~Ub and $Ube2H_{core}$~Ub, the rate of Ub transfer to lysine was enhanced in the presence of both MG53 constructs (Figure 2.11). In all cases, the rate of disappearance of the Ube2H~Ub band, as well as the rate of appearance of the Ube2H band, is enhanced by either

MG53 construct as compared to the no-E3 control. $MG53_{RBCC}$ increased aminolysis rates more than $MG53_{RING}$, so the presence of the B-box and coiled coil domains may be functionally important for either E3 ligase activity or Ube2H binding. $MG53_{RBCC}$ enhanced aminolysis equally well for $Ube2H_{FL}$ and $Ube2H_{core}$. In the context of the intrinsic reactivity assays, the C-terminal extension does not appear to be important for MG53-mediated lysine aminolysis. There is an important caveat in interpreting the results in Figure 2.11: it is possible that the apparent increase in lysine reactivity could be attributable to other phenomena besides MG53 binding to and activating Ube2H. For example, although E1 activity is quenched by the addition of EDTA in intrinsic reactivity assays, there is still detectable E1 activity during the timecourse of the experiment, so Ube2H~Ub conjugates that have transferred Ub to free lysine can then be recharged by E1. MG53 may have altered the rate of recharging by E1, leading to the apparent increased rate of lysine reactivity. I next sought to confirm binding between $Ube2H_{FL}$ and $MG53_{RBCC}$ given the promising enhancement of activity.

The binding experiments between $Ube2H_{FL}$ and $MG53_{RBCC}$ do not indicate high affinity binding (Figure 2.13). If the interaction were strong, the addition of 0.7 molar equivalents of $MG53_{RBCC}$ would be expected to result in either CSPs or intensity losses (broadening) across all peaks of the Ube2H spectrum, with more pronounced broadening for specific residues involved in the binding interaction. Instead, peaks broaden only moderately (as evidenced by I/Io values near 1), which is consistent with weak affinity binding. To determine if there are $Ube2H_{FL}$ peaks that specifically broaden to a greater extent than average, I calculated the ratio of intensities of each peak in the presence of $MG53_{RBCC}$ at both 0.3 and 0.7 molar equivalents to the apo state (I/Io) (Figure 2.13B). Interestingly, two C-terminal extension residues undergo significant broadening at both 0.3 and 0.7 molar equivalents $MG53_{RBCC}$ and therefore may be involved in the interaction

(S164 and S166). Intensity losses were plotted on a model of $Ube2H_{FL}$ to identify an $MG53_{RBCC}$ binding surface (Figure 2.13C). The most highly broadened residues do not form a distinct binding surface, as would be expected for a binding interaction. It is important to note that intensity loss measurements are often error-prone due to the fact that many peaks are not well-resolved from neighboring peaks. However, the fact that the same residues (Y99, F105, S164, S166) undergo the most significant broadening at both 0.3 and 0.7 molar equivalents $MG53_{RBCC}$, coupled with the fact that that the extent of broadening increases with the molar ratio of $MG53_{RBCC,}$ suggests that these residues are indeed specifically affected by the interaction.

A qualitative comparison of the spectra in the presence and absence of $MG53_{RBCC}$ shows evidence of a weak binding interaction, but the data do not clearly map to a distinct $MG53_{RBCC}$ binding surface on $Ube2H_{FL}$. The fact that peak broadening is weak even at 0.7 molar equivalents of $MG53_{RBCC}$ implies that if a binding interaction does occur, it is weak. There is evidence of an interaction between $MG53_{RBCC}$ and $Ube2H_{FL}$ from the enhanced biochemical activity in Figure 2.12, but binding does not necessarily need to be strong in order to observe enzymatic activity.

In all likelihood, $MG53_{RBCC}$ binds Ube2H in a manner similar to other TRIM E3 ligase-E2 interactions, where the N-terminal helix and nearby loops of the E2 are bound directly by the RING domain of the TRIM (see Figure 1.2). The binding residues identified in Figure 2.13 do not clearly map to the canonical E3-binding region of Ube2H, which is an indication that the intensity loss measurements are too insensitive to capture the interaction. Nonetheless, it is still possible that the C-terminal residues S164 an S166 could indeed contribute additional contacts in the interaction to mediate specificity in the Ube2H-MG53 interaction. To further characterize the interaction, N-terminal Ube2H residues should be assigned and additional titrations of MG53 constructs into ^{15}N-Ube2H should be performed to more carefully track which residues are selectively broadened.

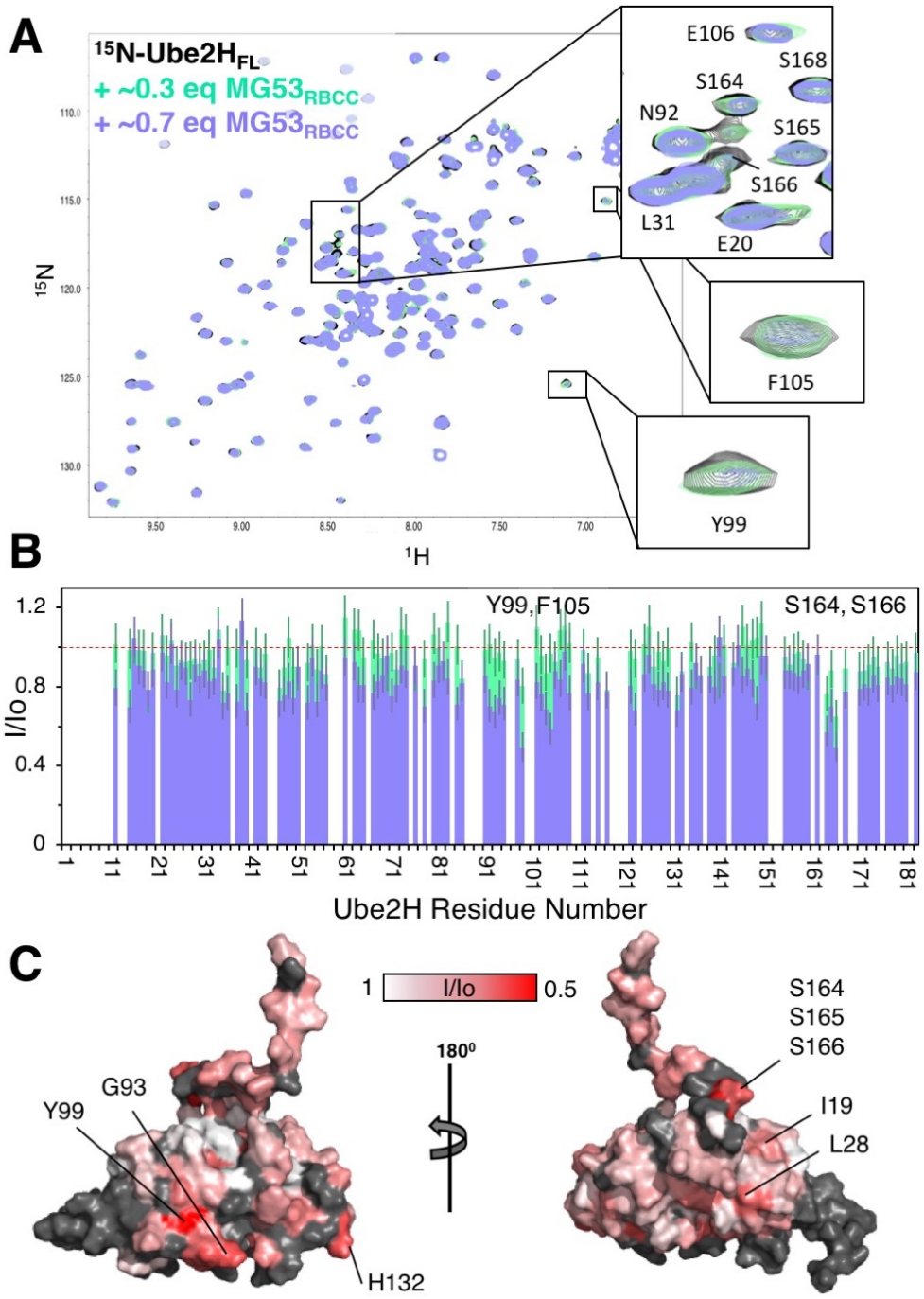

Figure 2.13. (A) Overlay of HSQC spectra of ^{15}N-Ube2H$_{FL}$ in the absence (black) and presence of MG53$_{RBCC}$ at 0.3 (teal) and 0.7 (lavender) molar equivalents. (B) Intensity losses (I/Io) plotted as a function of Ube2H$_{FL}$ residue number. Unassigned Ube2H$_{FL}$ residues are shown as blanks. Residues with the largest intensity losses are indicated. (C) Intensity losses for the 0.7 molar equivalents spectrum (lavender) are plotted on a model of Ube2H$_{FL}$ according to the indicated scale. Unassigned residues are shown in grey.

2.8 TRIM28 AND MAGEC2

TRIM28 is another TRIM E3 ligase that has been suggested to function with Ube2H *in vivo*. TRIM28 was reported to function with Ube2H in *in vitro* ubiquitylation assays, and the addition of the melanoma-associated antigen C2 (MAGEC2) enhanced the E3 ligase activity significantly (Doyle 2010). Given that Ube2H is capable of ubiquitylating H2B in the absence of an E3 (Figure 2.8), I tested whether TRIM28 and MAGEC2 enhanced the rate of H2B ubiquitylation by both $Ube2H_{FL}$ and $Ube2H_{core}$ (Figure 2.14).

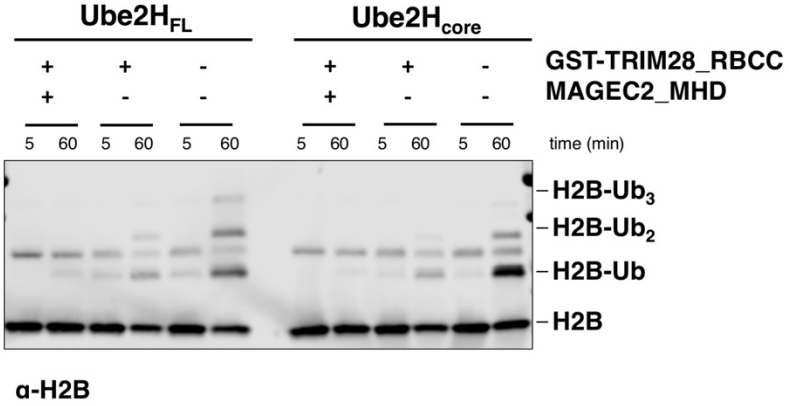

Figure 2.14. H2B ubiquitylation by $Ube2H_{FL}$ (left) and $Ube2H_{core}$ (right) in the absence and presence of $TRIM28_{RBCC}$ and $MAGEC2_{MHD}$. Products were detected by anti-H2B Western blot.

Surprisingly, H2B ubiquitylation is reduced rather than enhanced in the presence of the E3 TRIM28 and MAGEC2. The presence of TRIM28 reduces the amount of H2B-Ub formed for both $Ube2H_{FL}$ and $Ube2H_{core}$, and H2B ubiquitylation further decreases when MAGEC2 is present. In the presence of both TRIM28 and MAGEC2, more H2B remains unmodified. Interestingly, the same TRIM28 and MAGEC2 constructs used in these assays were shown to be active with Ube2H in p53 ubiquitylation *in vitro* (Doyle 2010), yet do not appear to stimulate H2B ubiquitylation.

Many TRIM E3 ligases form dimers or higher-order oligomers through the coiled-coil domain, and in some cases the catalytic RING domains are not functional as monomers. To address

a concern that the N-terminal GST-tag on $TRIM28_{RBCC}$ used in the Figure 2.13 assay may have enforced a dysfunctional oligomerization state of the TRIM28, I repeated the assay to test whether untagged TRIM28 enhances Ube2H-mediated H2B ubiquitylation (Figure 2.15).

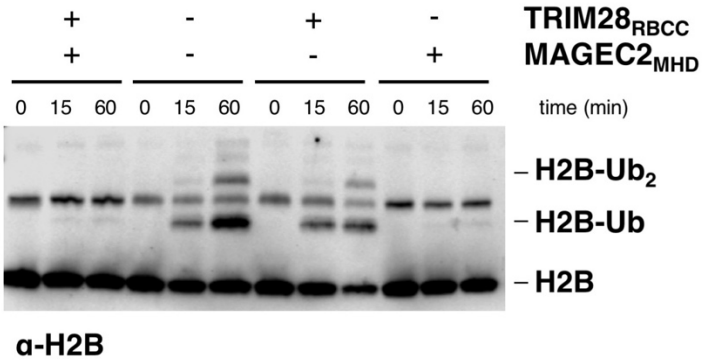

Figure 2.15. H2B ubiquitylation by $Ube2H_{FL}$ in the absence and presence of $TRIM28_{RBCC}$ and $MAGEC2_{MHD}$. Products were detected by anti-H2B Western blot.

Consistent with the results in Figure 2.14, $Ube2H_{FL}$-mediated H2B ubiquitylation is decreased in the presence of untagged $TRIM28_{RBCC}$ (Figure 2.15). Intriguingly, the presence of MAGEC2 alone is sufficient to ablate H2B ubiquitylation activity. The results in Figures 2.14 and 2.15 are surprising considering that TRIM28 and MAGEC2 have been shown to enhance Ube2H-mediated ubiquitylation of p53 (Doyle 2010). It is worth reiterating that neither H2B nor p53 are known to be bona fide Ube2H substrates *in vivo*. One possible explanation for the apparent discrepancy is that the H2B monomer is highly basic and charged. In particular, if either TRIM28 or MAGEC2 bind to or aggregate H2B, the effective concentration of H2B available to act as a Ube2H substrate would be reduced. Similarly, it is also possible that the presence of TRIM28 and MAGEC2 results in decreased H2B ubiquitylation because they bind to Ube2H in a manner that precludes Ube2H-H2B interactions, thereby sequestering enzyme that would otherwise be capable of ubiquitylation.

TRIM E3 ligases are notoriously complicated. The role of oligomerization in E3 ligase function is unclear, as is the role of regulation by post-translational modifications. Without a clear

in vitro ubiquitylation assay with which to probe the interactions between Ube2H, TRIM28, and MAGEC2, I turned my focus toward the novel interaction between Ube2H and MAGEC2.

Binding experiments between $Ube2H_{FL}$ and $MAGEC2_{MHD}$ suggest weak affinity binding. In the presence of 0.125 and 1.2 molar equivalents $MAGEC2_{MHD}$, there is no widespread, substantial broadening across all Ube2H peaks, and no CSPs occur. As with $MG53_{RBCC}$, intensity losses for Ube2H peaks were calculated, and residues with intensity losses were plotted on a model of $Ube2H_{FL}$ to identify specific residues that interact with $MAGEC2_{MHD}$. Ube2H's C-terminal extension does not appear to be involved in $MAGEC2_{MHD}$ binding, as none of the residues in the extension undergo significant broadening. UBC domain residues G40, F70, and H76 undergo the largest intensity losses, but they do not map to a distinct binding surface (Figure 2.16C). These residues are all buried in the UBC domain and therefore cannot be directly involved in binding interactions. Instead, these residues are likely affected allosterically by binding. H76 is a structurally important residue in the HPN motif (see Figure 1.2), and the specific broadening of this residue upon MAGEC2 binding may point toward a restructuring of the Ube2H catalytic cleft.

Notably, L98, D100, and N102 form a distinct surface adjacent to the N-terminal helix. Poor coverage in the N-terminal region of Ube2H precludes assessment of whether other residues also participate in an interaction with $MAGEC2_{MHD,}$ and further studies will be needed to determine if Ube2H's N-terminal helix is involved in $MAGEC2_{MHD}$ interactions.

Doyle et al. reported a binding interaction between tagged Ube2H and MAGEC2 via pull-down immunoprecipitation assays (Doyle 2010). The results in Figure 2.16 represent the first biophysical evidence of the interaction, supporting previous reports and providing residue-specific information regarding the interaction. Additional evidence of a MAGEC2-Ube2H interaction in a reconstituted ubiquitylation assay would lend support to the biophysical evidence provided here.

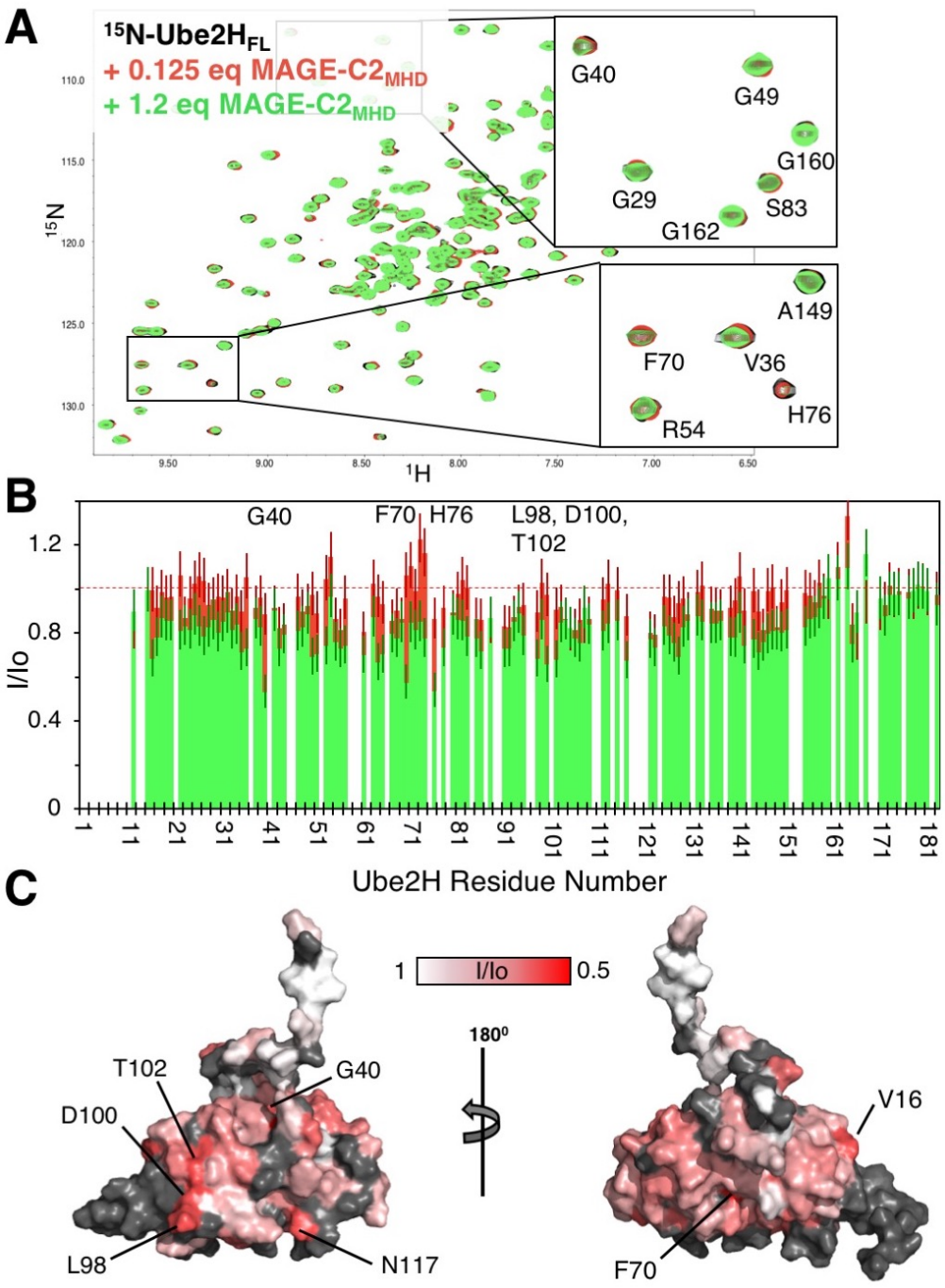

Figure 2.16. (A) Overlay of HSQC spectra of ^{15}N-Ube2H$_{FL}$ in the absence (black) and presence of MAGEC2$_{MHD}$ at 0.125 (red) and 1.2 (green) molar equivalents. (B) Intensity losses (I/Io) are plotted as a function of Ube2H$_{FL}$ residue number. Unassigned Ube2H$_{FL}$ residues are shown as blanks. Residues with the largest intensity losses are indicated. (C) Intensity losses for the 1.2 molar equivalents spectrum (green) are plotted on a model of Ube2H$_{FL}$ according to the indicated scale. Unassigned residues are shown in grey.

Chapter 3. CONCLUSION

3.1 CONCLUSION

Phylogenetic conservation analysis of Ube2H's C-terminal extension suggests that this domain likely performs some critical function in Ube2H biology. In this thesis, I assessed the structural and functional effects of deleting the extension as a means to gain insight into what role the extension might serve. In assays performed in the absence of E3s and substrates, there was no robust difference between the reactivities of $Ube2H_{FL}$ and $Ube2H_{core}$. However, NMR spectra collected on $Ube2H_{FL}$ and $Ube2H_{core}$ provided the insight that while the C-terminal extension is disordered, its presence has some effect on the chemical environment of several UBC core domain residues through an unknown mechanism. In particular, residues near the UBC domain N-terminus may interact transiently with the C-terminal extension. SAXS analysis of Ube2H-O-Ub oxyester conjugates suggested that in the presence of the C-terminal extension, the Ube2H~Ub conjugate may adopt a more open conformation. However, chemical shift perturbation mapping indicated that the C-terminal extension does not alter the chemical environment of Ub moieties in Ube2H~Ub conjugates. Consistent with the CSP mapping experiments, the presence of the C-terminal extension did not alter rates of lysine reactivity in ubiquitylation assays.

The biological role of Ube2H remains poorly understood, and it is difficult to determine the function of the C-terminal extension without a clear understanding of the function of Ube2H itself. It is possible that Ube2H may play a very specific role under specific conditions or contexts that have simply not been screened to date. Identification of functional, cognate E3 ligases would provide a crucial framework for investigating the function of the C-terminal extension. Although neither MG53 nor TRIM28 have been demonstrated to be bona fide ligases for Ube2H, there is at least some *in vivo* evidence to suggest they may be. In this thesis, I report *in vitro* evidence that

MG53 is a functional E3 ligase partner to Ube2H. Intrinsic reactivity of Ube2H~Ub conjugates was stimulated by the presence of MG53, and weak binding was observed between Ube2H and MG53. Intriguingly, several residues in Ube2H's C-terminal extension appear to be involved in MG53 binding. H2B ubiquitylation by Ube2H decreased in the presence of TRIM28 and its binding partner MAGEC2, contrary to expectations. Given that weak binding was observed between Ube2H and MAGEC2, it is possible that the confounding H2B ubiquitylation results could be explained by a non-enzymatic binding interaction. Specifically, binding between MAGEC2 and Ube2H could effectively reduce the affinity for Ube2H and H2B, thus decreasing rates of H2B ubiquitylation.

3.2 FUTURE DIRECTIONS

The observed binding between Ube2H and both MG53 and MAGEC2 represent an exciting opportunity to further characterize novel E2 interactions. In particular, structural characterization of the Ube2H-MAGEC2 interaction would constitute the first detailed report of an E2-MAGE interaction. MAGE proteins are known to function with specific E2 enzymes (Doyle 2010), so there are likely to be structural features that mediate such specificity. Further NMR binding titrations using different MAGEC2 constructs and point-mutants would provide insight into the binding interaction. In parallel, a functional ubiquitylation assay involving MAGEC2 should be established as a biochemical read-out of the Ube2H-MAGEC2 interaction.

Given the fact that deletion of the C-terminal tail does not result in changes to enzymatic activity in ubiquitylation assays, the C-terminal extension may not modulate intrinsic E2 activity, but may instead serve to mediate protein-protein interactions. Indeed, the observed binding interactions between Ube2H and $MG53_{RBCC}$ appear to involve C-terminal extension residues. This interaction will need to be confirmed in further biophysical and biochemical studies, including

binding experiments with point-mutants in C-terminal residues designed to disrupt binding. In addition, MG53 ubiquitylation assays such as intrinsic activity assays should be carried out in parallel to test the functional effects of binding interaction mutations.

Cognate E3 ligases and substrates must be established for Ube2H before the biochemistry of the system can be interrogated comprehensively. The ubiquitylation assays reported here represent first steps toward determining functional E3 ligases. The TRIM ligase truncation constructs used in the assays were selected based on previous reports, but may not be functionally folded or may lack domains that are necessary for adequate binding. Further work is needed to rigorously identify functional E3s as well as substrates. Detection of E3 autoubiquitylation in ubiquitylation assays would be an excellent read-out in confirming functional E3s. The reported p53 ubiquitylation by TRIM28-MAGEC2 may prove to be a useful *in vitro* ubiquitylation system for Ube2H. In addition to further validating TRIM28 and MG53, a yeast two-hybrid screen could be a useful approach in screening the multiple TRIM and RING E3s that have been reported to interact with Ube2H in high throughput screens (BioGrid, Oughtred 2019). Once functional E3 ligases and substrates are identified, the role of the C-terminal extension can be investigated in the context of cognate binding partners. Orthologs of Ube2H in model organisms such as *S. cerevisiae* and *C. elegans* could also provide an effective system for determining functional effects of C-terminal extension deletion *in vivo*. Once functional ligases and substrates for Ube2H are determined, structural characterization of the role Ube2H's disordered C-terminal tail promises to inform our understanding of E2 enzyme diversity.

Chapter 4. METHODS

Protein expression and purification

Ube2H constructs (WT, core, C87S) were expressed on a pET28a vector with a thrombin-cleavable N-terminal His_6-tag. Plasmids were transformed into *Escherichia coli* (BL21 DE3) cells in either LB media or minimal media supplemented with ^{15}N-ammonium chloride for NMR spectroscopy and cells were grown at 37 °C. Protein expression was induced at OD_{600} of 0.6 by addition of 0.2 mM IPTG and cells were grown at 16 °C for 16 hours. Cells were lysed by French press in 25 mM Tris-HCl, 200 mM NaCl, 10 mM imidazole, pH 7.6 and applied to gravity-flow Ni-NTA beads (GE Healthcare). Beads were washed with 25 mM Tris-HCl, 200 mM NaCl, 50 mM imidazole, pH 7.6 and subsequently eluted in 25 mM Tris-HCl, 200 mM NaCl, 500 mM imidazole, pH 7.6. The eluted His_6-tagged proteins were dialyzed in the presence of thrombin (1 mg) overnight at 4 °C into 25 mM Tris-HCl, 200 mM NaCl, pH 7.6. Dialysate was re-applied to Ni-NTA beads followed by thrombin capture beads. Flow-through was collected, concentrated, and applied to a gel filtration column (Supderdex 75, GE Healthcare) in 25 mM sodium phosphate, 150 mM NaCl, pH 7.0.

$MAGEC2_{MHD}$, $TRIM28_{RBCC}$, and $MG53_{RING}/MG53_{RBCC}$ were expressed from pGEX6p1 vectors with PreScission-cleavable N-terminal GST-tags. Plasmids were transformed into *Escherichia coli* (BL21 DE3) cells in LB and incubated at 37 °C. Protein expression was induced at OD_{600} of 0.6 by addition of 0.2 mM IPTG and incubated at 16 °C overnight. Cells were lysed by French press in 25 mM Tris-HCl, 150 mM NaCl, 1 mM DTT, pH 8.0 and applied to gravity-flow glutathione sepharose beads and washed with 25 mM Tris-HCl, 150 mM NaCl, 1 mM DTT, 0.1% TritonX100, pH 8.0. Beads were collected and incubated at 4 °C overnight with GST-tagged PreScission

protease for on-column GST-tag cleavage. The sample was re-applied to gravity flow and the flow-through was collected, concentrated, and applied to a gel filtration column (Superdex 75 for MAGEC2; Superdex 200 for TRIM28 and MG53, GE Healthcare) in 25 mM sodium phosphate, 150 mM NaCl, pH 7.0 (MAGEC2) or 20 mM HEPES, 100 mM NaCl, 1 mM DTT, pH 8.0 (TRIM28 and MG53).

Human E1 and Ub were purified as previously described (Pickart 2005).

Phylogenetic Conservation

The orthologs used for the ConSurf multiple sequence alignment were generated using a UniProt database and manually curated to exclude partial sequences and sequences from uncultured/environmental samples. Sequences were aligned using MAFFT. Conservation scores were weighted by phylogenetic distance using the default ConSurf algorithm. MODELLER was used to generate a model of full-length Ube2H based on the crystal structure of the Ube2H UBC domain. ConSurf was used to map conservation scores onto the Ube2H model structure.

Ubiquitylation Assays

E3-independent chain-building assays (Figure 2.6)

Human E1 (2 μM), $Ube2H_{FL}$ or $Ube2H_{core}$ (20 μM), Ub (60 μM) and $MgCl_2$/ATP (5 mM) were incubated in a total volume of 100 μL in 25 mM sodium phosphate, 150 mM NaCl, pH 7.0 at 37 °C for two hours. Timepoint samples (25 μL) were taken at 0, 1, and 2 hours after addition of $MgCl_2$/ATP and quenched in 2X SDS-PAGE non-reducing load dye on ice. Additionally, for final timepoints, samples (25 μL) were taken and quenched in 2X SDS-PAGE reducing load dye. Samples were run on 15% SDS-PAGE gels and stained by and visualized by Coomassie staining.

Intrinsic reactivity/lysine reactivity assays (Figure 2.7 and 2.12)

Thioester Ube2H~Ub conjugates were generated by incubating 30 μM $Ube2H_{FL}$ or $Ube2H_{core}$, 90 μM Ub,1 uM human E1, and 5 mM $MgCl_2$/ATP in a total volume of 100 μL in 25 mM sodium phosphate, 150 mM NaCl, pH 7.0 at 37 °C for one hour. Charging reactions were quenched by addition of 20 mM EDTA, and 40 mM lysine was added to initiate the assay for one hour. In MG53-mediated lysine reactivity assays, 4 μM MG53 was included with 40 mM lysine. Sample timepoints were removed from the reaction mixture and quenched in 2X SDS-PAGE non-reducing load dye on ice. Additionally, for final timepoints, samples (25 μL) were taken and quenched in 2X SDS-PAGE reducing load dye. Samples were run on 15% SDS-PAGE gels, and visualized by Coomassie staining. Gels were quantified using ImageJ.

H2B ubiquitylation assays (Figures 2.8, 2.14, and 2.15)

Human E1 (1 μM), $Ube2H_{FL}$ or $Ube2H_{core}$ (4 μM), Ub (20 μM), H2B (4 μM), and $MgCl_2$/ATP (5 mM) were incubated in a total volume of 100 μL in 25 mM sodium phosphate, 150 mM NaCl, pH 7.0 at 37 °C. For TRIM28-MAGEC2 H2B ubiquitylation assays, $MAGEC2_{MHD}$ (8 μM) and/or $TRIM28_{RBCC}$ (8μM) were included. Reactions were initiated by addition of ATP, and timepoint samples (10 μL) were removed from the reaction mixture and quenched in 2X SDS-PAGE reducing load dye. Samples were run on 15% SDS-PAGE gels, and visualized by Western blot using rabbit anti-H2B (abcam). Gels were quantified using ImageJ.

Generation of oxyester conjugates *(Figures 2.9, 2.10, and 2.11)*

Stable oxyester mimics of Ube2H~Ub conjugates were generated using purified active site mutants of both $Ube2H_{FL}$ and $Ube2H_{core}$ in which the active site cysteine was substituted for serine (C87S). Ube2H-O-Ub conjugates were charged by incubating 200 μM $Ube2H_{FL,C87S}$ or $Ube2H_{core,C87S}$ with 10 μM human E1, 1 mM Ub (Ub_{WT} for SAXS in Figure 2.10 or ^{15}N-Ub for NMR in Figure 2.9), and 10 mM ATP/$MgCl_2$ at 30 °C in 25 mM sodium phosphate, 150 mM NaCl, pH 7.0 for 10 hours. Ube2H-O-Ub conjugates were purified from other reaction components by multiple rounds of gel filtration (Superdex 75, GE Healthcare).

NMR Spectroscopy *(Figures 2.3, 2.4, 2.10, 2.11, 2.13, and 2.16)*

Two-dimensional ^{15}N, ^{1}H HSQC NMR experiments were performed on a 500 MHz Bruker Avance II spectrometer, and three-dimensional ^{13}C, ^{15}N, ^{1}H NMR spectra were collected on a 600 MHz Bruker Avance III spectrometer equipped with a cryoprobe. All data were processed using NMRPipe (Delaglio 1995). Residue-specific peak assignments were completed for both $Ube2H_{core}$ and $Ube2H_{FL}$ using NMRViewJ (Johnson 1994). Secondary structure propensities for C-terminal extension residues were calculated using the formula: propensity = $(C_{\alpha,measured} - C_{\alpha,randomcoil}) - (C_{\beta,measured} - C_{\beta,randomcoil})$. All HSQC spectra for Ube2H were recorded at 25 °C at 100 μM in 25 mM sodium phosphate, 150 mM NaCl, pH 7.0 in 10% D_2O. For binding experiments, unlabeled binding partner was added to samples at indicated molar equivalents. Peak intensities and chemical shifts were measured in NMRViewJ. Chemical shift perturbations were calculated using the formula: $\Delta\delta j = [(\Delta\delta j\ ^{15}N/5)^2 + (\Delta\delta j\ ^{1}H)^2]^{1/2}$. For binding experiments, intensities for each peak are reported as the fraction of intensity in the presence of binding partner to intensity of apo ^{15}N-Ube2H (I/I_0). Error in I/I_0 was calculated assuming 5% error in intensities for I_0 values. For HSQC

spectra of ^{15}N-Ub conjugated oxyesters (Ube2H$_{FL}$-O-^{15}N-Ub and Ube2H$_{core}$-O-^{15}N-Ub), peaks were analyzed for chemical shift perturbations as described above.

Small-Angle X-Ray Scattering (SAXS)

SAXS experiments were performed by at Stanford Synchrotron Radiation Lightsource (SSRL) beamline 4-2 with in-line gel filtration (SEC-SAXS). Ube2H constructs and oxyester-linked ubiquitin conjugates were each applied at concentrations of 5 and 10 mg/mL onto a Superdex 200 Increase PC 3.2/30 (GE) in 25 mM sodium phosphate, 150 mM NaCl, 0.02% NaN_3, pH 7.0 at 25 °C at a flow rate of 0.05 mL/min. Data were collected using a Pilatus3 X 1 M detector with a 2.5 m sample-to-detector discance and X-ray beam energy of 12.4 keV (λ = 1.127 Å) with 1-second exposures collected in 5-second increments. The first 100 data points during void volume elution were averaged and used as baseline buffer scattering data. Scattering data from the elution peaks were selected and background buffer scattering data was subtracted. The ATSAS software suite was used to analyze SAXS scattering curves, generate Kratky and P(r) plots, and calculate radius of gyration (R_g) and maximal particle dimension (D_{max}) (Franke 2017).

MODELLER was used to generate 100 models for Ube2H$_{FL}$~Ub and Ube2H$_{core}$~Ub conjugates using the crystal structure of Ube2H$_{core}$ (PDB 2Z5D) and Ub (PDB 1UBQ). The oxyester linkage was explicitly enforced in models and the C_α-C_α distance between the C-terminal ubiquitin backbone carbonyl and the active site serine sidechain oxygen of Ube2H restrained to 4.7 Å. The FOXS server was used to generate theoretical SAXS scattering curves for all models, and each model was fit to the corresponding experimental scattering curves to generate χ^2 values (Schneidman-Duhovny 2010). Structures of the ten best-fitting models were aligned by the Ube2H$_{core}$ domain for all constructs.

REFERENCES

Akimov V., Barrio-Hernandez I., Hansen S.V.F., Hallenborg P., Pedersen A-K., Bekker-Jensen D.B., Puglia M., Christensen S.D.K., Vanselow J.T., Nielsen M.M., Kratchmarova I., Kelstrup C.D., Olsen J.V., and Blagoev B. (2018) UbiSite approach for comprehensive mapping of lysine and N-terminal ubiquitination sites. *Nature Structural Molecular Biology.* **25,** 631-640.

Ashkenazy H., Abadi S., Martz E., Chay O., Mayrose I., Pupko T., and Ben-Tal N. (2016). ConSurf 2016: an improved methodology to estimate and visualize evolutionary conservation in macromolecules. *Nucleic Acids Research*. **44**, W344-W350.

Blom, N., Gammeltoft S., and Brunak S. (1999). Sequence and structure-based prediction of eukaryotic protein phosphorylation sites. *Journal of Molecular Biology*. **294**, 1351-1362.

Brzovic PS, Lissounov A, Christensen DE, Hoyt DW, and Klevit RE. (2006). A UbcH5/ubiquitin noncovalent complex is required for processive BRCA1-directed ubiquitination. *Molecular Cell.* **21,** 873-880.

Delaglio F., Grzesiek S, Vuister GW, Zhu G, Pfeifer J, Bax A.. (1995) NMRPipe: a multidimensional spectral processing system based on UNIX pipes. *Journal Biomolecular NMR*. **6**, 277-293.

Dickinson ME, Flenniken AM, Ji X, Teboul L, Wong MD, White JK, Meehan TF, Weninger WJ, Westerberg H, Adissu H, Baker CN, Bower L, Brown JM, Caddle LB, Chiani F, Clary D, Cleak J, Daly MJ, Denegre JM, Doe B, Dolan ME, Edie Helmut Fuchs SM, Gailus-Durner V, Galli A, Gambadoro A, Gallegos J, Guo S, Horner NR, Hsu CW, Johnson SJ, Kalaga S, Keith LC, Lanoue L, Lawson TN, Lek M, Mark M, Marschall S, Mason J, McElwee ML, Nutter SNLMJ, Peterson KA, Ramirez-Solis R, Rowland DJ, Ryder E, Samocha KE, Seavitt JR, Selloum M, Szoke-Kovacs Z, Tamura M, Trainor AG, Tudose I, Wakana S, Warren J, Wendling O, West DB, Wong L, Yoshiki A; International Mouse Phenotyping Consortium, Wurst W, MacArthur DG, Tocchini-Valentini GP, Gao X, Flicek P, Bradley A, Skarnes WC, Justice MJ, Parkinson HE, Moore M, Wells S, Braun RE, Svenson KL, de Angelis MH, Herault Y, Mohun T, Mallon AM, Henkelman RM, Brown SDM, Adams DJ, Lloyd KCK, McKerlie C, Beaudet AL, Murray MBSA. (2017). Corrigendum: High-throughput discovery of novel developmental phenotypes. *Nature*. **537,** 508-514.

Doyle JM, Gao J, Wang J, Yang M, and Potts PR. (2010). MAGE-RING protein complexes comprise a family of E3 ubiquitin ligases. *Molecular Cell.* **39,** 963-974.

Drozdetskiy, A., Cole, C., Procter, J., and Barton, G.J. (2015). JPred4: a protein secondary structure prediction server. *Nucleic Acids Research*. **43**, W389-W394.

Emanuelsson O, Nielsen H, Brunak S, von Heijne G. (2000). Predicting subcellular localization of proteins based on their N-terminal amino acid sequence. *Journal Molecular Biology*. **300,** 1005-1016.

Franke D, Petoukhov MV, Konarev PV, Panjkovich A, Tuukkanen A, Mertens HDT, Kikhney AG, Hajizadeh NR, Franklin JM, Jeffries CM, Svergun DI. (2017). ATSAS 2.8: a comprehensive data analysis suite for small-angle scattering from macromolecular solutions. *Journal Applied Crystallography*. **50**, 1212-1225.

Gauci S., Helbig A.O., Slijper M., Krijgsveld J., Heck A.J.R., and Mohammed S. (2009). Lys-N and trypsin cover complementary parts of the phosphoproteome in a refined SCX-based approach. *Analytical Chemistry*. **81,** 4493-501.

Hornbeck P.V., Zhang B., Murray B., Kornhauser J.M., Latham V., and Skrzypek E. (2015). PhosphoSitePlus, 2014: mutations, PTMs and recalibrations. *Nucleic Acids Research.* **43**, D512-20.

Johnson BA, Blevins RA. (1994) NMR View: A computer program for the visualization and analysis of NMR data. *Journal Biomolecular NMR*. **4**, 603-614.

Kaiser P, Seufert W, Höfferer L, Kofler B, Sachsenmaier C, Herzog H, Jentsch S, Schweiger M, and Schneider R. (1994). A human ubiquitin-conjugating enzyme homologous to yeast UBC8. *Journal of Biological Chemistry*. **269,** 8797-8802.

Kaiser P, Mandl S, Schweiger M, and Schneider R. (1995). Characterization of functionally independent domains in the human ubiquitin conjugating enzyme UbcH2. *FEBS Letters*. **377,** 193-196.

Kleiger G, Hao B, Mohl DA, Deshaies RJ. (2009). The acidic tail of the Cdc34 ubiquitin-conjugating enzyme functions in both binding to and catalysis with ubiquitin ligase SCFCdc4. *Journal Biological Chemistry*. **139,** 957-968.

Komander D, and Rape M. (2012). The ubiquitin code. *Annual Review Biochemistry.* **81,** 203-229.

Lampert F, Stafa D, Goga A, Soste MV, Gilberto S, Olieric N, Picotti P, Stoffel M, and Peter M. (2018). The multi-subunit GID/CTLH E3 ubiquitin ligase promotes cell proliferation and targets the transcription factor Hbp1 for degradation. *Elife*. **7,** e35528.

Lausen J, Pless O, Leonard F, Kuvardina ON, Koch B, Leutz A. (2010). Targets of the Tal1 transcription factor in erythrocytes: E2 ubiquitin conjugase regulation by Tal1. *Journal Biological Chemistry*. **285,** 5338-5346.

Lee CS, Yi JS, Jung SY, Kim BW, Lee NR, Choo HJ, Jang SY, Han J, Chi SG, Park M, Lee JH, and Ko YG. (2010). TRIM72 negatively regulates myogenesis via targeting insulin receptor substrate-1. *Cell Death Differentiation.* **17,** 1254-1265.

Lindskog C, Mardinoglu A, Ponten F. (2017). A pathology atlas of the human cancer transcriptome. *Science*. **357,** eaan2507.

Malec V., Coulson J.M., Urbé S., Clague M.J. (2015). Combined Analyses of the VHL and Hypoxia Signaling Axes in an Isogenic Pairing of Renal Clear Cell Carcinoma Cells. *Journal of Proteome Research.* **14**, 5263-72.

Middleton AJ, Day CL. (2015). The molecular basis of lysine 48 ubiquitin chain synthesis by Ube2K. *Scientific Reports*. **5,** 16793.

Middleton AJ, Wright JD, Day CL. (2017). Regulation of E2s: A Role for Additional Ubiquitin Binding Sites? *Journal Molecular Biology*. **429,** 3430-3440.

Miller, M. L., Jensen, L. J., Diella, F., Jørgensen, C., Tinti, M., Li, L., Hsiung, M., Parker, S. A., Bordeaux, J., Sicheritz-Ponten, T., Olhovsky, M., Pasculescu, A., Alexander, J., Knapp, S., Blom, N., Bork, P., Li, S., Cesareni, G., Pawson, T., Turk, B. E., Yaffe, M. B., Brunak, S., and Linding, R. (2008). Linear motif atlas for phosphorylation-dependent signaling. *Science Signaling*. **35**, ra2.

Minard, A.Y., Tan, S-X., Yang, P., Fazakerley, D.J., Domanova, W., Parker, B.L., Humphrey, S.J., Jothi, R., Stöckli, J., and James, D.E. (2016). mTORC1 Is a Major Regulatory Node in the FGF21 Signaling Network in Adipocytes. *Cell Reports*. **17**, 29-36.

Nguyen N, Yi JS, Park H, Lee JS, and Ko YG. (2014). Mitsugumin 53 (MG53) ligase ubiquitinates focal adhesion kinase during skeletal myogenesis. *Journal Biological Chemistry*. **289,** 3209-3216.

Oughtred R, Stark C, Breitkreutz BJ, Rust J, Boucher L, Chang C, Kolas N, O'Donnell L, Leung G, McAdam R, Zhang F, Dolma S, Willems A, Coulombe-Huntington J, Chatr-Aryamontri A, Dolinski K, Tyers M. (2019). The BioGRID interaction database: 2019 update. *Nucleic Acids Research*. **47,** D529-D541.

Pickart CM, CM, Raasi S. (2005). Controlled synthesis of polyubiquitin chains. *Methods Enyzmology.* **399**, 21-36.

Pinto S.M., Nirujogi R.S., Rojas P.L., Patil A.H., Manda S.S., Subbannayya Y., Roa J.C., Chatterjee A., Prasad T.S., and Pandey A. (2015). Quantitative phosphoproteomic analysis of IL-33-mediated signaling. *Proteomics*. **15**, 532-44.

Povlsen, L.K., Beli P., Wagner S.A., Poulsen S.L., Sylvestersen K.B., Poulsen J.W., Nielsen M.L., Bekker-Jensen S., Mailand N., and Choudhary C. (2012). Systems-wide analysis of ubiquitylation dynamics reveals a key role for PAF15 ubiquitylation in DNA-damage bypass. *Nature Cell Biology.* **14**, 1089-98.

Qin S, Nakajima B, Nomura M, and Arfin SM. (1991). Cloning and characterization of a Saccharomyces cerevisiae gene encoding a new member of the ubiquitin-conjugating protein family. *Journal Biological Chemistry*. **266,** 15549-15554.

Santt O, Pfirrmann T, Braun B, Juretschke J, Kimmig P, Scheel H, Hofmann K, Thumm M, and Wolf DH. (2008). The yeast GID complex, a novel ubiquitin ligase (E3) involved in the regulation of carbohydrate metabolism. *Molecular Biology Cell*. **19,** 3323-3333.

Schelpe J, Monté D, Dewitte F, Sixma TK, and Rucktooa P. (2016). Structure of UBE2Z Enzyme Provides Functional Insight into Specificity in the FAT10 Protein Conjugation Machinery. *Journal Biological Chemistry*. **291,** 630-639.

Schneidman-Duhovny D, Hammel M, Tainer JA, and Sali A. (2016). FoXS, FoXSDock and MultiFoXS: Single-state and multi-state structural modeling of proteins and their complexes based on SAXS profiles. *Nucleic Acids Research*. **44,** W424-429.

Schüle T, Rose M, Entian KD, Thumm M, and Wolf DH. (2000). Ubc8p functions in catabolite degradation of fructose-1, 6-bisphosphatase in yeast. *EMBO*. **19,** 2161-2167.

Schumacher FR, Wilson G, and Day CL. (2013). The N-terminal extension of UBE2E ubiquitin-conjugating enzymes limits chain assembly. *Journal Molecular Biology.* **425,** 4099-4111.

Sheng, Y., Hong, J.H., Doherty, R., Srikumar, T., Shloush, J., Avvakumov, G.V., Walker, J.R., Xue, S., Neculai, D., Wan, J.W., Kim, S.K., Arrowsmith, C.H., Raught, B., and Dhe-Paganon, S. (2012). A Human Ubiquitin Conjugating Enzyme (E2)-HECT E3 Ligase Structure-function Screen. *Molecular Cellular Proteomics*. **11**, 329-341.

Stewart MD, Ritterhoff T, Klevit RE, Brzovic PS. (2016). E2 enzymes: more than just middle men. *Cell Research*. **26,** 423-440.

Thompson O, Edgley M, Strasbourger P, Flibotte S, Ewing B, Adair R, Au V, Chaudhry I, Fernando L, Hutter H, Kieffer A, Lau J, Lee N, Miller A, Raymant G, Shen B, Shendure J, Taylor J, Turner EH, Hillier LW, Moerman DG, Waterston RH. (2013). The million mutation project: a new approach to genetics in Caenorhabditis elegans. *Genome Research.* **23,** 1749-1762.

Thul PJ, Åkesson L, Wiking M, Mahdessian D, Geladaki A, Ait Blal H, Alm T, Asplund A, Björk L, Breckels LM, Bäckström A, Danielsson F, Fagerberg L, Fall J, Gatto L, Gnann C, Hober S, Hjelmare M, Johansson F, Lee S, Lindskog C, Mulder J, Mulvey CM, Nilsson P, Oksvold P, Rockberg J, Schutten R, Schwenk JM, Sivertsson Å, Sjöstedt E, Skogs M, Stadler C, Sullivan DP, Tegel H, Winsnes C, Zhang C, Zwahlen M, Mardinoglu A, Pontén F, von Feilitzen K, Lilley KS, Uhlén M, Lundberg E. (2017). A subcellular map of the human proteome. *Science.* **356,** eaal3321.

Uhlén M, Fagerberg L, Hallström BM, Lindskog C, Oksvold P, Mardinoglu A, Sivertsson Å, Kampf C, Sjöstedt E, Asplund A, Olsson I, Edlund K, Lundberg E, Navani S, Szigyarto CA, Odeberg J, Djureinovic D, Takanen JO, Hober S, Alm T, Edqvist PH, Berling H, Tegel H, Mulder J, Rockberg J, Nilsson P, Schwenk JM, Hamsten M, von Feilitzen K, Forsberg M, Persson L, Johansson F, Zwahlen M, von Heijne G, Nielsen J, Pontén F. (2015). Tissue-based map of the human proteome. *Science*. **347,** 1260419.

Uhlén M, Zhang C, Lee S, Sjöstedt E, Fagerberg L, Bidkhori G, Benfeitas R, Arif M, Liu Z, Edfors F, Sanli K, von Feilitzen K, Oksvold P, Lundberg E, Hober S, Nilsson P, Mattsson J, Schwenk JM, Brunnström H, Glimelius B, Sjöblom T, Edqvist PH, Djureinovic D, Micke P,

Verano-Braga T., Schwämmle V., Sylvester M., Passos-Silva D.G., Peluso A.A.B., Etelvino G.M., Santos R.A.S., and Roepstorff P. (2012). Time-resolved quantitative phosphoproteomics: new insights into Angiotensin-(1-7) signaling networks in human endothelial cells. *Journal of Proteomics Research* **11,** 3370-81.

Vourc'h P, Martin I, Bonnet-Brilhault F, Marouillat S, Barthélémy C, Pierre Müh J, Andres C. (2003). Mutation screening and association study of the UBE2H gene on chromosome 7q32 in autistic disorder. *Psychiatric Genetics*. **13,** 221-225.

Wagner, S. A., Beli, P., Weinert, B. T., Nielsen, M. L., Cox, J., Mann, M., & Choudhary, C. (2011). A proteome-wide, quantitative survey of in vivo ubiquitylation sites reveals widespread regulatory roles. *Molecular Cellular Proteomics*. **10,** M111.013284.

Wagner, S. A., Beli, P., Weinert, B. T., Schölz, C., Kelstrup, C. D., Young, C., Nielsen, M. L., Olsen, J. V., Brakebusch, C., and Choudhary, C. (2012). Proteomic analyses reveal divergent ubiquitylation site patterns in murine tissues. *Molecular Cellular Proteomics*. **11,** 1578-85.

Wang C, Ivanov A, Chen L, Fredericks WJ, Seto E, Rauscher FJ, Chen J. (2005). MDM2 interaction with nuclear corepressor KAP1 contributes to p53 inactivation. *EMBO*. **24,** 3279-3290.

Webb B., and Sali A. (2016). Comparative Protein Structure Modeling Using MODELLER. *Current Protocols in Bioinformatics*. **54**, 5.6.1-5.6.37.

Wenzel DM, Lissounov A, Brzovic PS, and Klevit RE. (2011). UBCH7 reactivity profile reveals parkin and HHARI to be RING/HECT hybrids. *Nature*. **474,** 105-108.

Wu PY, Hanlon M, Eddins M, Tsui C, Rogers RS, Jensen JP, Matunis MJ, Weissman AM, Wolberger C, Pickart CM. (2003). A conserved catalytic residue in the ubiquitin-conjugating enzyme family. *EMBO*. **22,** 5241-5250.

Yi JS, Park JS, Ham YM, Nguyen N, Lee NR, Hong J, Kim BW, Lee H, Lee CS, Jeong BC, Song HK, Cho H, Kim YK, Lee JS, Park KS, Shin H, Choi I, Lee SH, Park WJ, Park SY, Choi CS, Lin P, Karunasiri M, Tan T, Duann P, Zhu H, Ma J, and Ko YG. (2013). MG53-induced IRS-1 ubiquitination negatively regulates skeletal myogenesis and insulin signalling. *Nature Communications*. **4,** 2354.

Zheng, N., and Shabek, N. (2017). Ubiquitin Ligases: Structure, Function, and Regulation. *Annual Review Biochemistry.* **86,** 129-15.